The Astrophysical Journal, 705:936–961, 2009 November 1 doi:10.1088/0004-637X/705/1/936

UV CONTINUUM SLOPE AND DUST OBSCURATION FROM $z \sim 6$ TO $z \sim 2$: THE STAR FORMATION RATE DENSITY AT HIGH REDSHIFT*

R. J. Bouwens[1,2], G. D. Illingworth[1], M. Franx[2], R.-R. Chary[3], G. R. Meurer[4], C. J. Conselice[5], H. Ford[4], M. Giavalisco[6], and P. van Dokkum[7]

[1] Astronomy Department, University of California, Santa Cruz, CA 95064, USA
[2] Leiden Observatory, University of Leiden, Postbus 9513, 2300 RA Leiden, Netherlands
[3] Divison of Physics, Mathematics, and Astronomy, California Institute of Technology, Pasadena, CA 91125, USA
[4] Department of Physics and Astronomy, Johns Hopkins University, 3400 North Charles Street, Baltimore, MD 21218, USA
[5] University of Nottingham, School of Physics & Astronomy, Nottinghm NG7 2RD, UK
[6] Department of Astronomy, University of Massachusetts, Amherst, MA, USA
[7] Department of Astronomy, Yale University, New Haven, CT, USA
Received 2009 May 28; accepted 2009 September 23; published 2009 October 16

ABSTRACT

We provide a systematic measurement of the rest-frame UV continuum slope β over a wide range in redshift ($z \sim 2$–6) and rest-frame UV luminosity (0.1 $L^*_{z=3}$ to 2 $L^*_{z=3}$) to improve estimates of the star formation rate (SFR) density at high redshift. We utilize the deep optical and infrared data (Advanced Camera for Surveys/NICMOS) over the Chandra Deep Field-South and Hubble Deep Field-North Great Observatories Origins Deep Survey fields, as well as the UDF for our primary $UBVi$ "dropout" Lyman Break Galaxy sample. We also use strong lensing clusters to identify a population of very low luminosity, high-redshift dropout galaxies. We correct the observed distributions for both selection biases and photometric scatter. We find that the UV-continuum slope of the most luminous galaxies is substantially redder at $z \sim 2$–4 than it is at $z \sim 5$–6 (from ~ -2.4 at $z \sim 6$ to ~ -1.5 at $z \sim 2$). Lower luminosity galaxies are also found to be bluer than higher luminosity galaxies at $z \sim 2.5$ and $z \sim 4$. We do not find a large number of galaxies with β's as red as -1 in our dropout selections at $z \sim 4$, and particularly at $z \gtrsim 5$, even though such sources could be readily selected from our data (and also from Balmer Break Galaxy searches at $z \sim 4$). This suggests that star-forming galaxies at $z \gtrsim 5$ almost universally have very blue UV-continuum slopes, and that there are not likely to be a substantial number of dust-obscured galaxies at $z \gtrsim 5$ that are missed in "dropout" searches. Using the same relation between UV-continuum slope and dust extinction as has been found to be appropriate at both $z \sim 0$ and $z \sim 2$, we estimate the average dust extinction of galaxies as a function of redshift and UV luminosity in a consistent way. As expected, we find that the estimated dust extinction increases substantially with cosmic time for the most UV luminous galaxies, but remains small ($\lesssim 2$ times) at all times for lower luminosity galaxies. Because these same lower luminosity galaxies dominate the luminosity density in the UV continuum, the overall dust extinction correction remains modest at all redshifts and the evolution of this correction with redshift is only modest. We include the contribution from ultra-luminous IR galaxies in our SFR density estimates at $z \sim 2$–6, but find that they contribute only $\sim$20% of the total at $z \sim 2.5$ and $\lesssim$10% at $z \gtrsim 4$.

Key words: galaxies: evolution – galaxies: high-redshift

1. INTRODUCTION

Quantifying the star formation rate (SFR) density at $z \gtrsim 3$ is a challenging endeavor. While there are a wide variety of techniques to estimate this rate at $z \lesssim 2$ from light at different wavelengths (Condon 1992; Kennicutt 1998; Madau et al. 1998; Ranalli et al. 2003; Yüksel et al. 2008; Li 2008; Reddy et al. 2006; Yun et al. 2001; Reddy & Steidel 2004; Reddy et al. 2006; Erb et al. 2006b), the situation becomes considerably more uncertain at redshift $z \gtrsim 3$. This is because most of the techniques effective at low redshifts rely upon light at wavelengths that simply cannot be detected at high redshifts for all but the most exceptional sources. Determinations of the SFR density from X-ray or radio emission appear to be just possible at $z \sim 2$–4 by stacking a large number of sources in very deep integrations (e.g., Seibert et al. 2002; Nandra et al. 2002; Reddy & Steidel 2004), but do not work at $z \geqslant 5$ (Lehmer et al. 2005; Carilli et al. 2008). Similarly, while deep mid-IR data would seem to be quite effective in estimating the SFR at $z \sim 2$ (e.g., Reddy et al. 2006; Caputi et al. 2007), at $z \geqslant 3$ many of the key spectral features redshift to wavelengths not very amenable to study with current instrumentation.

This leaves us with sparingly few techniques for estimating the SFR density at high redshift, most of which have only recently been developed. These techniques include traditional approaches like a consideration of the UV light to estimate the SFR densities to newer approaches that use gamma-ray burst (GRB) rate densities (e.g., Yüksel et al. 2008; Li 2008) or possible detections of redshifted Hα (e.g., Chary et al. 2005) to make these estimates.

Perhaps, the simplest and most practical of these techniques is to rely on the UV light emanating from the high-redshift galaxies themselves. Young stars emit a large fraction of their energy at these wavelengths, and it is very easy using current instrumentation to measure this energy to very low SFR rates (i.e., $\sim$0.1 $M_\odot$ yr^{-1} at $z \sim 4$ in the Hubble Ultra Deep Field (HUDF; Beckwith et al. 2006)). One of the most significant challenges in establishing the SFR from the UV data is estimating the absorption by dust. Since UV light is subject to substantial attenuation by dust, this entire issue is quite

* Based on observations made with the NASA/ESA *Hubble Space Telescope*, which is operated by the Association of Universities for Research in Astronomy, Inc., under NASA contract NAS 5-26555. These observations are associated with programs 7235, 7817, 9425, 9575, 9797, 9803, 9978, 9979, 10189, 10339, 10340, 10403, 10504, 10530, 10632, 10872, 10874, 11082, and 11144.

important. One of the most practical methods for determining the dust attenuation is through the UV-continuum slopes β ($f_\lambda \propto \lambda^\beta$). Since these slopes have been shown to be well correlated with the dust extinction at $z \sim 0$ (Meurer et al. 1995, 1997, 1999; Burgarella et al. 2005; Dale et al. 2007; Treyer et al. 2007; Salim et al. 2007), $z \sim 1$ (Laird et al. 2005), and $z \sim 2$ (Reddy et al. 2006; Daddi et al. 2004), we can use these slopes to estimate the dust obscuration at even higher redshift.

Not surprisingly, there have already been a number of attempts to determine these slopes at high redshifts ($z \sim 2$–6) from the available imaging data. Adelberger & Steidel (2000) and Meurer et al. (1999) examined the UV slopes for a sample of $z \sim 3$ U-dropouts and inferred modest (factor of $\sim$5) dust extinctions. Other groups (Lehnert & Bremer 2003; Ouchi et al. 2004; Stanway et al. 2005; Yan et al. 2005; Bouwens et al. 2006) have looked at these slopes at higher redshifts ($z \sim$4–6), again based on a dropout selection. Broadly, it was found that higher redshift galaxies had bluer UV-continuum slopes than lower redshift galaxies have, suggesting that the typical dust extinction at high redshift is significantly less than it is at lower redshift. There was also some evidence from previous analyses (e.g., Meurer et al. 1999 at $z \sim 2.5$) that lower luminosity galaxies had bluer UV-continuum slopes β and thus lower dust extinctions (though the emphasis in Meurer et al. 1999 was the correlation between β and the dust-corrected luminosity, not the observed luminosity).

Regrettably, apart from these two trends (higher redshift galaxies are bluer and lower luminosity galaxies are bluer), it has been difficult to make quantitative statements about the distribution of UV-continuum slopes or dust extinctions for galaxies at high redshift. In part, this can be attributed to the piecemeal way the UV-continuum slopes and dust extinction have been derived at high redshift, as different analyses have derived UV-continuum slopes based upon a wide variety of disparate high-redshift galaxy samples, using different techniques (not all of which are consistent). In part, this can also be attributed to the limited amounts of data available to each particular study. Fortunately, the situation has begun to change, and there is now a wide variety of *Hubble Space Telescope* (*HST*) data that are available to select high-redshift galaxies and determine their slopes over a wide range in redshift and luminosity. Determining how these slopes also depend upon luminosity seems particularly relevant given the fact that these sources likely dominate the UV luminosity density and perhaps SFR density at $z \gtrsim 2$ (e.g., Bouwens et al. 2006; Sawicki & Thompson 2006b; Bouwens et al. 2007; Reddy et al. 2008; Yan & Windhorst 2004; Reddy & Steidel 2009).

It seems clear that a comprehensive, systematic determination of the distribution of UV-continuum slopes is needed, both as a function of redshift and luminosity. The goal of the present paper is to provide just such an analysis, taking advantage of the considerable quantity of deep *HST* data to clarify our understanding of dust obscuration and, by consequence, the SFR density at high redshift. We select galaxies for UV-continuum slope measurements over a wide range in redshift using well-tested $z \sim 2.5$ U, $z \sim 4$ B, $z \sim 5$ V, and $z \sim 6$ i dropout selections. We use the wide-area Advanced Camera for Survey (ACS) Great Observatories Origins Deep Survey (GOODS) fields (Giavalisco et al. 2004a) to quantify these slopes at bright magnitudes and extend our analyses to very low luminosities by examining very deep *HST* data sets like the HUDF, and also by examining dropouts behind massive galaxy clusters where the substantial magnification factors permit us to consider very faint sources.

The plan for this paper is as follows. In Section 2, we present the observational data set. In Section 3, we describe our procedure for generating source catalogs from these data, selecting the dropout samples, and estimating the UV-continuum slopes while correcting for the effect of object selection and photometric scatter. Finally, we discuss our results (Section 4), examine the likely implications of these results for the effective dust extinction and SFR density at $z \sim 2$–6 (Sections 5 and 6), and then include a summary (Section 7). Throughout this work, we will find it convenient to quote results in terms of the luminosity $L^*_{z=3}$ Steidel et al. (1999) derived at $z \sim 3$, i.e., $M_{1700,AB} = -21.07$, for consistency with previous work—though we note that the Steidel et al. (1999) luminosity function (LF) results are now updated ($M_{1700,AB} = -20.97 \pm 0.14$; Reddy & Steidel 2009) but still consistent with the previous determination. Where necessary, we assume $\Omega_0 = 0.3$, $\Omega_\Lambda = 0.7$, $H_0 = 70\,\mathrm{km\,s^{-1}\,Mpc^{-1}}$. Although these parameters are slightly different from those determined from the *WMAP* five-year results (Dunkley et al. 2009), they allow for convenient comparison with other recent results expressed in a similar manner. Unless otherwise stated, the UV-continuum slope β presented here all assume a 1600–2300 Å baseline. We express all magnitudes in the AB system (Oke & Gunn 1983).

2. OBSERVATIONAL DATA

The purpose of this study is to measure the UV-continuum slope over as wide a range in luminosity and redshift as is practical from current observations. Of course, establishing this distribution even over a limited range in redshift or luminosity can be a challenge, as it requires very deep imaging over a wide wavelength range, both to select galaxies through the Lyman break technique and to measure their UV-continuum slope redward of this break. It also requires sufficient search area to provide a sufficiently large samples of sources to effectively define the distribution of UV-continuum slopes.

At $z \sim 2.5$, we use the deep U-band coverage available over the WFPC2 Hubble Deep Field (HDF)-North (Williams et al. 1996) and HDF-South (Casertano et al. 2000) to select $z \sim 2.5$$U$-dropouts. Those two deep WFPC2 fields are invaluable for defining the distribution of UV-continuum slopes at lower luminosities, but their small area limits their value for establishing the distribution at the higher luminosities. However, as we will see, the UV-continuum slope distribution for bright $z \sim 2.5$ galaxies is similar to what Adelberger & Steidel (2000) and Reddy et al. (2008) derived previously. For our $z \sim 4$ B, $z \sim 5$ V, and $z \sim 6$ i-dropout samples, we utilize the ACS $B_{435}V_{606}i_{775}z_{850}$ data available over the HUDF, HUDF05 (Oesch et al. 2007; Bouwens et al. 2007), and GOODS fields. The wide-area GOODS fields are used for establishing the UV-continuum slope distribution for luminous galaxies while the deeper HUDF and HUDF05 fields are used for establishing the UV-continuum slope distribution for lower luminosity galaxies. The reduction of these latter data was performed with *"apsis"* (Blakeslee et al. 2003) and is described in Bouwens et al. (2006, 2007). A summary of the properties of these fields is given in Table 1.

Importantly, the HUDF, HUDF05, and GOODS fields also have $\sim$70 arcmin^2 of very deep near-IR coverage with NICMOS—reaching 5σ limits of $\gtrsim$26.5 (0.″6-diameter apertures). This coverage is important for measurements of the UV-continuum slope β for galaxies in our $z \sim 5$ V-dropout and $z \sim 6$ i-dropout selections. The NICMOS data are described in more detail in R. J. Bouwens et al. (2009, in preparation) and

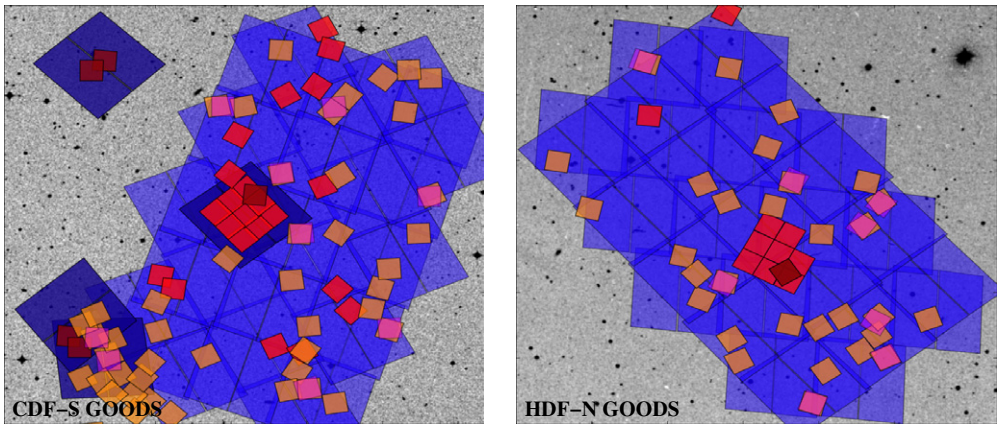

Figure 1. Illustration of the deep near-IR data available over the two GOODS fields. Deep near-IR data are essential for measurements of the UV-continuum slope of galaxies at $z \gtrsim 5$ and valuable for a measurement of these slopes at $z \sim 4$. The red and dark red regions correspond to regions with deep and very deep NICMOS J_{110} and H_{160} coverage, respectively (5σ depths $\gtrsim 26.5$ and $\gtrsim 28$ AB mag). The light orange regions have deep NICMOS H_{160}-band coverage (5σ depths of $\gtrsim 26.5$; H. Teplitz et al. 2009, in preparation; C. Conselice et al. 2009, in preparation) while the magenta regions have deep NICMOS J_{110}-band coverage (5σ depths of $\gtrsim 26.5$; R.J. Bouwens et al. 2009, in preparation). The blue and dark blue regions correspond to regions with deep and very deep optical ACS $V_{606}i_{775}z_{850}$ coverage, respectively (5σ depths of $\gtrsim 28$ and $\gtrsim 29$ AB mag). For more details on the NICMOS data over the two GOODS fields, see Bouwens et al. (2008) and R. J. Bouwens et al. (2009, in preparation).

Table 1
Observational Data Used to Select $z \sim$ 2–6 *U*-, *B*-, *V*-, and *i*-Dropouts and to Measure the UV-Continuum Slope

Field	Optical		z_{850}-Band	Near-IR		H_{160}-Band
	Passbands	Area[a]	5σ Limit[b]	Passbands	Area[a]	5σ Limit[b]
HDF-N	$U_{300}B_{450}V_{606}I_{814}$	5	27.6	$J_{110}H_{160}$	5	27.3
HDF-S	$U_{300}B_{450}V_{606}I_{814}$	4	28.0	...	...	...
GOODS	$B_{435}V_{606}i_{775}z_{850}$	316	27.4	$J_{110}H_{160}$	18	26.4
GOODS	...	...	...	H_{160}	36	26.4
HUDF05	$B_{435}V_{606}i_{775}z_{850}$	22	28.4	$J_{110}H_{160}$	2.5	28.6
HUDF	$B_{435}V_{606}i_{775}z_{850}$	11	28.8	$J_{110}H_{160}$	6	27.2
Abell 2218	$g_{475}r_{625}i_{775}z_{850}$	11	27.2	$J_{110}H_{160}$	1.5	26.8
MS1358	$g_{475}r_{625}i_{775}z_{850}$	11	27.2	$J_{110}H_{160}$	1.5	26.8
CL0024	$g_{475}r_{625}i_{775}z_{850}$	11	27.2	$J_{110}H_{160}$	3.0	26.8
Abell 1689	$g_{475}r_{625}i_{775}z_{850}$	11	27.2	...[c]	...	...
Abell 1703	$g_{475}r_{625}i_{775}z_{850}$	11	27.2	...[c]	...	...

Notes.
[a] arcmin^2
[b] 5σ point-source limiting magnitude in 0.″6 diameter apertures.
[c] While NICMOS J_{110} observations are available over both Abell 1689 and Abell 1703, these clusters lack deep coverage at $\sim$1.6 μm and so we do not make use of the existing NICMOS data to measure UV-continuum slopes β for $z \sim 5$ *V*-dropout or $z \sim 6$ *i*-dropout selections.

are illustrated in Figure 1(see also Bouwens et al. 2008). These data were obtained as a result of the cumulative observations of many different *HST* programs (e.g., Dickinson 1999; Thompson et al. 1999, 2005; Bouwens et al. 2005; Oesch et al. 2007; Riess et al. 2007; C. Conselice et al. 2009, in preparation). All the NICMOS data taken since 2002 (when the NICMOS cryocooler went into operation) were reduced with our NICMOS pipeline *"nicred.py"* (Magee et al. 2007).

Finally, we take advantage of the deep *HST* data over three massive galaxy clusters to identify a small number of lower luminosity star-forming galaxies at $z \sim$ 4–6 behind these clusters. Because of lensing by the foreground cluster (magnifying faint $z \sim$ 5–6 galaxies by factors of $\gtrsim 4$), it is possible to select and to measure UV-continuum slopes for a small number of extremely low luminosity galaxies. The five galaxy clusters (MS1358, CL0024, Abell 2218, Abell 1689, Abell 1703) all have deep ACS $B_{435}g_{475}V_{555}r_{625}i_{775}z_{850}$ data and cover 55 arcmin^2 in total. These clusters also have 6 arcmin^2 of deep $J_{110}H_{160}$ NICMOS data necessary to measure the UV-continuum slope for $z \sim 5$ *V* dropout and $z \sim 6$ *i*-dropout galaxies behind these clusters. The ACS data available over these clusters were also reduced with *"apsis"* while the NICMOS data were reduced with *"nicred.py"*. These reductions are described in more detail in Bouwens et al. (2009a) and Zheng et al. (2009).

3. ANALYSIS

In this section, we describe our procedure for determining the distribution of UV-continuum slopes β from our observational data as a function of redshift and UV luminosity. We begin by discussing how we do photometry on our observational data and then select $z \sim$ 2–6 galaxies using various dropout criteria (Sections 3.1–3.2). In Section 3.3, we calibrate our optical/near-IR photometry and then derive UV-continuum slopes from the measured colors (Section 3.4). By combining measurements of the UV-continuum slope determinations from both very deep and wide-area data sets, we derive the UV-continuum slope distribution over a wide range in luminosity (Section 3.5). In Section 3.6, we take advantage of lensing from massive galaxy clusters to examine the UV-continuum slope β distribution for a set of lower luminosity galaxies. We correct the observed distributions of UV-continuum slopes β for the effect of object selection and photometric scatter (Section 3.7). Finally, we discuss the uncertainties that likely exist in our determinations (Section 3.8) and then give our final estimates of the UV-continuum slope distributions in Section 3.9.

3.1. Photometry

We used SExtractor (Bertin & Arnouts 1996) to perform object detection and photometry. Object detection was performed using the square root of the χ^2 images (Szalay et al. 1999; essentially a co-addition of the relevant images) constructed from all ACS images with coverage redward of the dropout band (e.g., $V_{606}i_{775}z_{850}$ in the case of a B_{435}-dropout selection) or the WFPC2 images redward of the dropout band in the case of our U_{300} dropout selection (where the $B_{450}V_{606}I_{814}$ bands are used).

For clarity, the χ^2 image is equal to

$$\Sigma_k (I_k(x, y)/N_k)^2,$$

where $I_k(x, y)$ is the intensity of image I_k at pixel (x, y), where N_k is the rms noise on that image, and where the index k runs over all the relevant images (i.e., those redward of the dropout band).

Our procedure for measuring colors depends upon the point-spread function (PSF) of the data we are using. For colors that include only the ACS or WFPC2 bands (where the PSF is much sharper than for NICMOS), we measure these colors in scalable apertures determined using a Kron (1980) factor of 1.2. When measuring colors that include the NICMOS near-IR bands, we first PSF match the ACS/WFPC2 data to the NICMOS H_{160}-band. Then, we use the same apertures described above if the area in those apertures is $\geqslant 0.38$ arcsec^2 (i.e., $\geqslant 0\farcs7$-diameter apertures). This only applies for the largest sources in our selection. Otherwise (and in most cases), the colors are measured in fixed $0\farcs7$-diameter apertures.

We correct the fluxes measured in the above apertures (used for color measurements) to total fluxes using a two-step procedure. First, the individual flux measurements are corrected to a much larger scalable aperture (using a Kron factor of 2.5). These corrections are made on a source-by-source basis using the square root of the χ^2 image (Szalay et al. 1999). Second, a correction is made to account for the light outside of these larger apertures and on the wings of the ACS Wide Field Camera (WFC) PSF (Sirianni et al. 2005). Typical corrections are $\sim$0.6 mag for the first step and $\sim$0.1–0.2 mag for the second step. While there are modest uncertainties in these corrections (typically 0.2 mag), these corrections only affect the total magnitude measurements and do not affect the colors.

3.2. Sample Selection

We select star-forming galaxies over the redshift range $z \sim 6$ to $z \sim 2$ using the well-established dropout technique (e.g., Steidel et al. 1996; Bunker et al. 2003; Vanzella et al. 2006, 2009; Dow-Hygelund et al. 2007; Stanway et al. 2007). Our U-dropout criterion is similar to those used by Bouwens et al. (2003) while our B, V, and i dropout criteria are almost identical to those adopted by Bouwens et al. (2007) except that our V-dropout criterion uses a sharper $(i_{775} - z_{850}) < 0.6$ cut to exclude dusty $z \sim 1$ interlopers. These criteria are

$$(U_{300} - B_{450} > 1.1) \wedge (B_{450} - I_{814} < 1.5)$$
$$\wedge (U_{300} - B_{450} > 0.66(B_{450} - I_{814}) + 1.1)$$

for our U-dropout sample

$$(B_{435} - V_{606} > 1.1) \wedge (B_{435} - V_{606} > (V_{606} - z_{850}) + 1.1)$$
$$\wedge\ (V_{606} - z_{850} < 1.6)$$

for our B-dropout sample,

$$[(V_{606} - i_{775} > 0.9(i_{775} - z_{850})) \vee (V_{606} - i_{775} > 2)]$$
$$\wedge (V_{606} - i_{775} > 1.2) \wedge (i_{775} - z_{850} < 0.6)$$

for our V-dropout sample, and

$$(i_{775} - z_{850} > 1.3) \wedge ((V_{606} - i_{775} > 2.8) \vee (\mathrm{S/N}(V_{606}) < 2))$$

for our i-dropout sample, where $\wedge$ and $\vee$ represent the logical AND and OR symbols, respectively, and S/N represents the signal-to-noise ratio. These criteria are illustrated in two color diagrams in Figure 2 and are very similar to those considered by Giavalisco et al. (2004b) and Beckwith et al. (2006).

To ensure that our selections did not contain any spurious sources, we required that sources in our U, B, V, and i dropout selections be $\geqslant 5.5\sigma$ detections in the I_{814}, z_{850}, z_{850}, and z_{850} bands, respectively. We inspected all sources in our dropout samples by eye to purge them of any obvious contaminants (diffraction spikes, irregularities in the background). Pointlike sources (SExtractor stellarity S/G >0.8) were also removed ($\lesssim 2\%$ of the relevant sources).

3.3. Calibration of the NICMOS Magnitudes

To accurately estimate the UV-continuum slopes β for galaxies in our sample, it is absolutely essential that the colors that we measure are accurate. For example, for a source with UV colors measured across the baseline 1600–2300 Å, a 0.1 mag error in this color translates into an error of 0.3 in the estimated slope β.

Measuring colors to this level of accuracy is challenging for a number of reasons, particularly in the near-IR. First and foremost, the NICMOS detector (essential for measuring the fluxes of faint sources in the near-IR) has been shown to suffer from significant nonlinearity in its count rate. While there are now procedures (e.g., de Jong et al. 2006) to correct for these nonlinearities, as utilized here, it is unlikely that the corrections are perfect in the magnitude range we are considering. This is because there are comparatively few deep fields available where the near-IR fluxes can be measured and calibrated against other data. Second, the colors we measure are derived from both optical (ACS) and near-IR (NICMOS) data where the PSF is very different. While such differences can be effectively addressed by carefully matching the PSFs of the two data sets before measuring fluxes (as we do here), PSF matching can be challenging to perform perfectly and so it is easy to introduce small systematic errors at this stage.

As a result of these issues, we took great care in deriving correction factors that we could apply to the measured NICMOS near-IR fluxes. For simplicity, we assumed that these correction factors did not depend on the luminosity of the sources we were considering—but rather were simple offsets we could add to the measured magnitudes. We established these correction factors by examining the photometry of a sample ($\sim$50) of relatively faint ($22 < z_{850,AB} < 26$) point-like stars (SExtractor stellarity >0.8) over the HUDF/GOODS fields, and then compared their observed colors with that expected from the Pickles (1998) atlas of stellar spectra. Given the very limited range in spectral energy distribution (SED) shape found in real stars, these comparisons should allow us to make reasonable corrections to the J- and H-band photometries. We determined the average differences between the measured and best-fit near-IR fluxes (both in the J_{110} and H_{160} bands) and found corrections of -0.13 mag and -0.07 mag for the J_{110} and H_{160} bands, respectively.

To ensure that these corrections were as accurate as possible, we also identified a sample of $\sim$60 highest S/N B-dropouts from our search fields (GOODS and HUDF) and then fit their observed SEDs with Bruzual & Charlot (2003) τ models. Since the 1.1 μm J- and 1.6μm H-band fluxes of these galaxies probe the light blueward of the age sensitive break at 3600 Å (probing 2300 Å and 3300 Å rest frame, respectively), it should be reasonable to use the available i (1600 Å rest frame) and z-band (1900 Å rest frame) fluxes to establish a UV-continuum slope β and extrapolate to these redder wavelengths. For our

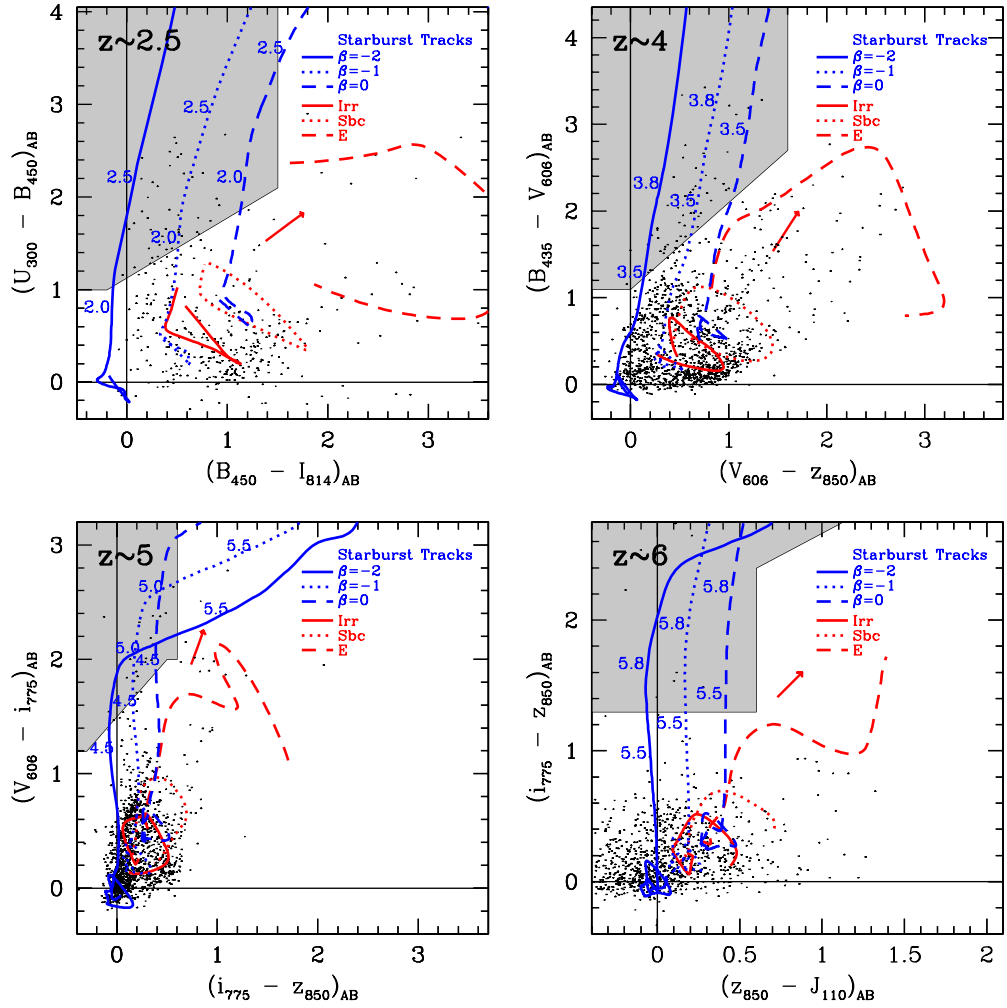

Figure 2. Two-color diagrams showing the selection criteria (see Section 3.2) we use to find $z \sim 2.5$ U, $z \sim 4$ B, $z \sim 5$ V, and $z \sim 6$ i dropouts in our search fields (upper left, upper right, lower left, and lower right panels, respectively). Sources that fall within the shaded regions would be included in our selections. The blue tracks show the expected colors of starbursts with different UV-continuum slopes as a function of redshift, while the red lines show the colors of low-redshift interlopers (Coleman et al. 1980). The black points illustrate the range of colors that real sources in our search fields possess. To ensure that these plotted distributions of colors are as realistic as possible, we only include sources from our deepest fields (the HDFs for our U-dropout selection and HUDF for our B-, V-, and i-dropout selection) and at relatively bright magnitudes ($I < 26$ for our U-dropout selection, $z < 26.5$ for our B-dropout selection, and $z < 27$ for our V-, i-dropout selections). The red arrows show the Calzetti et al. (2000) reddening vectors. These diagrams show that our selection criteria are effective in identifying high-redshift galaxies with UV-continuum slopes β bluer than 0.5, but less effective in identifying galaxies redward of this limit (Figures 4 and 6 show the effective selection volume calculated to be available to galaxies with various UV-continuum slopes).

fiducial model-fit parameters, we assumed a $e^{-t/\tau}$ star formation history (with $t = 70$ Myr, $\tau = 10$ Myr), a Salpeter initial mass function (IMF), and $[Z/Z_{\odot}] = -0.7$, and let the dust extinction and redshift be free parameters (the fiducial model considered by Papovich et al. 2001 in their stellar population modeling of $z \sim 3$ U-dropouts). Comparing the predicted near-IR fluxes (from the models) with the measured fluxes, we computed corrections to the J- and H-band fluxes. The corrections were -0.08 ± 0.02 mag and 0.04 ± 0.2 mag, respectively (the uncertainties were derived using other SED models (the Appendix) to determine these corrections). Because of the size of the uncertainties in the H-band corrections (from the $z \sim 4$ B-dropouts), we gave those results very low weight overall for the H-band correction.

Combining the constraints we derived from our sample of stars and $z \sim 4$ Lyman Break Galaxies (LBGs)—which were consistent within 0.05 mag—we derived a -0.10 mag correction to the measured J_{110}-band magnitudes. For the NICMOS H_{160}-band, we derived a -0.05 mag correction from the above fits—using the SED fit results to stars as our primary constraint.[8] The measured J_{110}- and H_{160}-band fluxes were therefore somewhat too faint (before correction). A brief discussion of the effect that uncertainties in the photometry/zero points could have on our derived UV-continuum slopes β is given in Section 3.8.

3.4. Measuring the UV-Continuum Slope β

Our principal interest is to determine the rest-frame UV-continuum slope β for the galaxies in our dropout samples. As noted in the introduction, the UV-continuum slope β specifies how the flux density of a galaxy varies with wavelength (i.e., $f_{\lambda} \propto \lambda^{\beta}$) in the UV-continuum (i.e., from ~1300 Å to ~3500 Å).

We estimate the UV-continuum slopes β from the broadband colors available for each galaxy in our sample. To make our

[8] We have subsequently verified that the corrections we derive here are very similar ($\lesssim 0.04$ mag) to what we derive matching sources in the HUDF with both NICMOS and WFC3/IR data (e.g., Bouwens et al. 2009b).

Table 2
Wavebands Used to Derive the UV Continuum Slope for Individual Galaxies in High-redshift *U*-, *B*-, *V*-, and *i* Dropout Samples[a,b]

Dropout Sample	Mean Redshift	Filters used for β determination	
		Lower	Upper
U-dropout	2.5	V_{606} (1730 Å)	I_{814} (2330 Å)
B-dropout	3.8	i_{775} (1610 Å)	z_{850} (1940 Å)
V-dropout	5.0	z_{850} (1550 Å)	$(J_{110} + H_{160})/2$ (2250 Å)
V-dropout	5.0	z_{850} (1550 Å)	H_{160} (2660 Å)
i-dropout	5.9	J_{110} (1570 Å)	H_{160} (2290 Å)

Notes.
[a] See Section 3.4 for discussion on the filter choices.
[b] Throughout this work, our β measurements are based upon the relationship $f_\lambda \propto \lambda^\beta$. Since real spectra will not have perfect power-law SEDs (and therefore depend upon the rest-frame wavelengths used to estimate β), small corrections are made to the estimated β's based upon a fiducial starburst SED ($e^{-t/\tau}$ star formation history with $t = 70$ Myr, $\tau = 10$ Myr, $[Z/Z_\odot] = -0.7$; from Papovich et al. 2001). See Section 3.4 and the Appendix for details. The filters that define the wavelength range of the β measurements for our different dropout samples are presented here.

Table 3
Dropout Samples Used to Measure the Distribution of UV-Continuum Slopes β as a Function of Redshift and UV Luminosity

Dropout Sample	Field	Luminosity Range[a]	No. of Sources
U-dropout	HDF-North	$-22 < M_{UV,AB} < -18$	97
	HDF-South	$-22 < M_{UV,AB} < -18$	71
B-dropout	GOODS-North	$-23 < M_{UV,AB} \lesssim -20.5$	218
	GOODS-South	$-23 < M_{UV,AB} < -20.5$	251
	HUDF	$-20.5 < M_{UV,AB} < -17$	470
	Cluster	$-23 < M_{UV,AB} \lesssim -20.5$	195
V-dropout	GOODS-North	$-23 < M_{UV,AB} \lesssim -20.0$	22
	GOODS-South	$-23 < M_{UV,AB} \lesssim -20.0$	19
	HUDF	$-23 < M_{UV,AB} \lesssim -19.5$	10
	HUDF05	$-23 < M_{UV,AB} \lesssim -19.5$	16
	Cluster	$-23 < M_{UV,AB} \lesssim -20.0$	12
i-dropout	GOODS-North	$-23 < M_{UV,AB} \lesssim -20.5$	2
	GOODS-South	$-23 < M_{UV,AB} \lesssim -20.5$	2
	HUDF	$-23 < M_{UV,AB} \lesssim -20.0$	5
	HUDF05	$-23 < M_{UV,AB} \lesssim -20.0$	3
	Cluster	$-23 < M_{UV,AB} \lesssim -20.5$	2

Note.
[a] Luminosity limits for $z \sim 4$ *B*-dropout samples are chosen to minimize the effects of photometry scatter and selection on the UV-continuum slope distribution. Luminosity limits for $z \sim 5$ *V*-dropout and $z \sim 6$ *i*-dropout samples are set according to the depth of the near-IR NICMOS data (see Section 3.5).

estimates of these slopes as uniform as possible, we selected filters at each redshift where the rest-frame UV wavelengths were as very close to 1650 Å and 2300 Å as possible. Of course, the actual effective wavelengths of these filters will vary somewhat from sample to sample—depending on the passbands in which broadband imaging is available for our different samples or the precise redshift of specific galaxies in our samples. Fortunately, the wavelength range 1650–2300 Å is a good match to the wavelength range used for studies of the dust extinction in galaxies at $z \sim 0$ (e.g., Meurer et al. 1995, 1999; Burgarella et al. 2005). Table 2 summarizes the passbands we use to probe these wavelengths for each of our dropout samples.

Some additional clarification may be helpful regarding specific filter choices. For our *B*-dropout sample, for example, we use the $i_{775} - z_{850}$ colors for these estimates to take advantage of the much higher quality (deeper, wider area) ACS data available. For our *V*-dropout sample, we use $z_{850} - (J_{110} + H_{160})/2$ colors predominantly for these estimates, but we also make use of $z_{850} - H_{160}$ colors for these estimates to take advantage of the large areas within the GOODS fields which have only NICMOS H_{160}-band coverage (primarily from the C. Conselice et al. 2009, in preparation, NICMOS program; see the light orange squares in Figure 1).

In principle, deriving the UV-continuum slopes β from the measured UV colors is straightforward. One simply takes power-law spectra $f_\lambda \propto \lambda^\beta$, calculates their colors at the mean redshift of each of our dropout samples, and then determines for which β the model spectrum reproduces the observed colors. In practice, however, since the spectrum of star-forming galaxies in the UV-continuum is not expected to be a perfect power law (as noted above), small differences in the wavelength range over which the UV-continuum slope β is measured will have an effect of the derived results.

To correct for these passband and wavelength-dependent effects, we base our estimates of β on a small number of more realistic SEDs calculated from stellar population models (Bruzual & Charlot 2003). These model SEDs are calibrated to have UV-continuum slopes β of -2.2, -1.5, and -0.8 over the wavelength range and assume a $e^{-t/\tau}$ star formation history ($t = 70$ Myr, $\tau = 10$ Myr, $[Z/Z_\odot] = -0.7$) with varying amounts of dust extinction calculated according to the Calzetti et al. (2000) law. The formulae we use to convert between the measured colors and the UV-continuum slope β are presented in the Appendix. The formulae we use to do the conversion depend somewhat on the star formation history assumed and likely result in an additional uncertainty in the derived UV-continuum slopes β of $\sim$0.1–0.2.

3.5. Constructing the UV-Continuum Slope Distribution from Multiple (Deep or Wide-area) Dropout Selections

In order to accurately quantify the distribution of UV-continuum slopes β over a wide range in luminosity, we alternatively used our deepest selections and our wide-area selections. We used the deepest selections to define the UV-continuum slope distribution at the lowest luminosities to maximize the S/N on the derived colors (while minimizing the importance of selection effects). Meanwhile, we used our widest area selections to define this distribution at higher luminosities. This allowed us to find a sufficient number of sources to map out the distribution of UV-continuum slopes (which is helpful for determining the mean and 1σ scatter). In Table 3, we provide a list of the fields we use to quantify the distribution of UV-continuum slopes at a given luminosity and redshift.

In Figure 3, we plot the UV-continuum slopes β observed for galaxies in our four dropout samples versus their UV luminosities. The mean UV-continuum slope β and 1σ for galaxies is also included in this figure (blue squares) as a function of luminosity for each of the dropout samples. We adopt finer 0.5 mag bins for our *B*-dropout selections than the 1.0 mag bins we adopt for our *U* and *V* dropout selections or 2.0 mag bins we adopt for our *i* dropout selection. The width of the bins depends upon the number of sources present in each of our dropout selections. The UV luminosity as shown on this diagram is the geometric mean of the two UV luminosities used to establish the UV slope (see Table 2). Use of the geometric mean of the two UV luminosities is preferred here for examining the

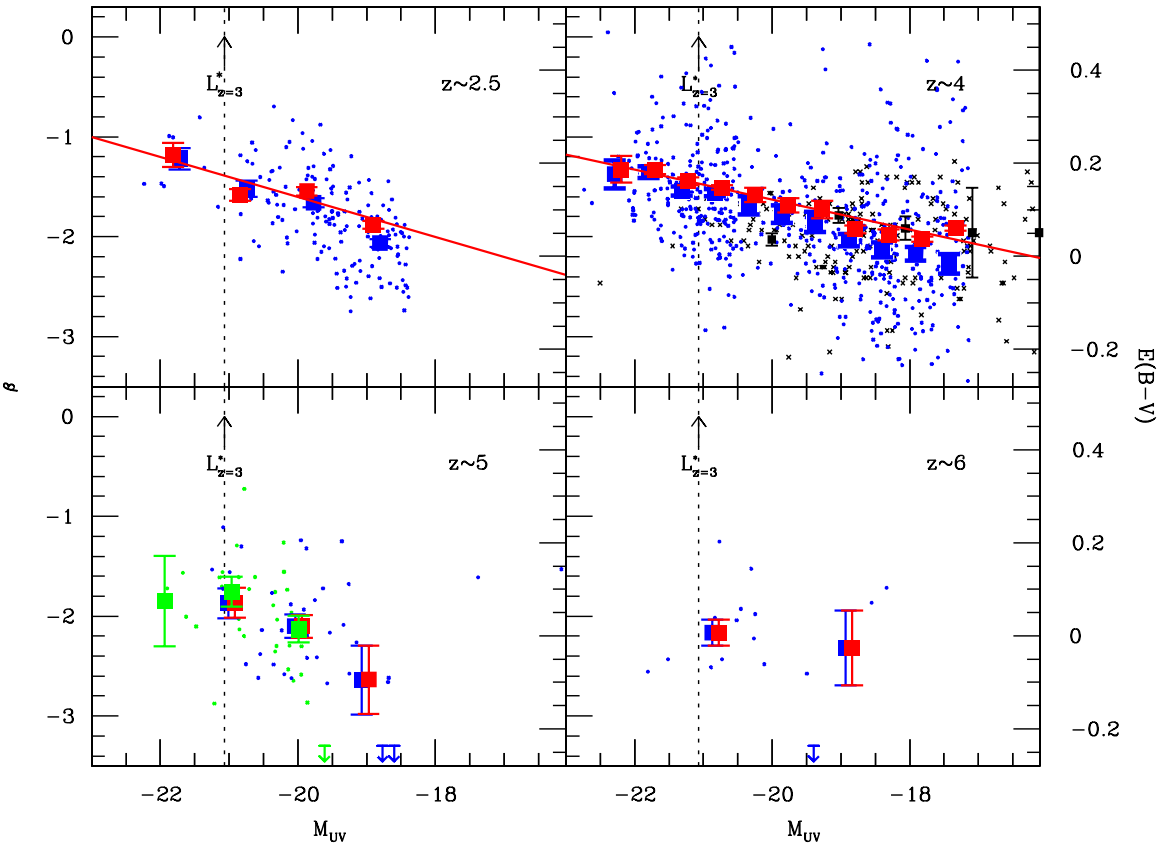

Figure 3. Determinations of the UV-continuum slope β (1600–2300 Å) vs. rest-frame UV luminosity for the present selection of $z \sim 2.5$ U, $z \sim 4$ B, $z \sim 5$ V, and $z \sim 6$ i dropouts. The UV luminosity here is the geometric mean of the UV luminosities measured in the bands used to establish the UV slope (see Table 2). On the right axes are the equivalent $E(B-V)$ extinctions (Calzetti et al. 2000 law) to a given β if the base spectrum is a young star-forming galaxy (~100 Myr of constant star formation)—which is only $\Delta E(B-V) = 0.02$ bluer than our fiducial τ model (i.e., the one referred to in footnote b of Table 2). The small points represent the UV-continuum slopes measured for individual galaxies in our samples while the open blue squares and vertical bars show the mean UV-continuum slope β and 1σ scatter (shown in a darker blue in the $z \sim 4$ panel for clarity). Blue upper limits are shown for a few $z \sim 5$ and $z \sim 6$ sources with β's bluer than -3.5. The green points on the $z \sim 5$ panel show the UV-continuum slope determinations derived from our V-dropout samples where only NICMOS H_{160}-band data are available (i.e., with no deep NICMOS J_{110}-band coverage). The black points on the $z \sim 4$ panel show the UV-continuum slope determinations derived from our B-dropout samples behind lensing clusters (where we have corrected their luminosities for model lensing magnification factors; see Section 3.6). It is encouraging that the UV-continuum slopes we derive from both of the latter V- and B-dropout selections agree with the determinations derived from our primary selections. The open red squares and vertical bars show the mean UV-continuum slope and 1σ error in this slope, after correcting for the effect of object selection and photometric scatter (Section 3.7). See Table 4 for a tabulation of these slopes. The red lines show the best-fit relationship between UV-continuum slope and the observed magnitude of a galaxy in the UV (see Sections 3.9 and 4.5). It is also clear that the UV-continuum slope β of star-forming galaxies is much redder at higher luminosities than it is at lower luminosities (particularly at $z \sim 2.5$ and $z \sim 4$).

correlation of β with luminosity since it allows us to evaluate the correlation without introducing any artificial correlations. Had we, for example, elected to use the bluer bands for examining this correlation, the UV-continuum slope β would be bluer as a function of the bluer-band luminosity, simply as a result of our examining the relationship as a function of this quantity. A similar (but opposite) bias would be introduced, in examining the UV-continuum slope β as a function of the redder band.

A clear trend is seen toward bluer UV-continuum slopes β at lower luminosities. This trend is similar to that found by Meurer et al. (1999) in their analyses of $z \sim 2.5$ U-dropout galaxies in the HDF North and also noted by Overzier et al. (2008) in their analysis of $z \sim 4$ g-dropouts in the TN1338 field (Figure 4 from that work).

3.6. UV-Continuum Slopes Derived for $z \sim 4$–6 Galaxies Gravitationally Lensed By Galaxy Clusters

In Section 3.5, we considered galaxies from both wide-area and deep surveys to establish the distribution of UV-continuum slopes β over a wide range in luminosity. We can increase the number of sources in our lower luminosity $z \sim 4$–6 samples, by considering gravitationally lensed sources behind high-redshift galaxy clusters. The clusters under consideration include Abell 2218, MS1358, CL0024, Abell 1689, and Abell 1703, and all allow us to select very faint star-forming galaxies at $z \sim 4$–6 from the available *HST* ACS data.

These clusters substantially amplify the flux from distant galaxies, making it possible to measure the UV-continuum slope of galaxies at lower luminosities than would otherwise be possible. Of course, in the case of B-dropout selections from very deep optical data like HUDF, we are able to reach to the same intrinsically luminosities as we reach in the B-dropout samples we compile from searches behind lensing clusters. We correct the luminosities of the dropout galaxies identified behind these clusters by applying gravitational lensing models from the literature. For Abell 2218, MS1358, CL0024 (sometimes known as CL0024+1652), Abell 1689, and Abell 1703, we adopt the models constructed by Elíasdóttir et al. (2007), Franx et al. (1997), Jee et al. (2007), Limousin et al. (2007), and Limousin et al. (2008), respectively. Typical magnification factors for the $z \sim 4$–6 galaxies we find behind galaxy clusters are ~ 5–10. We

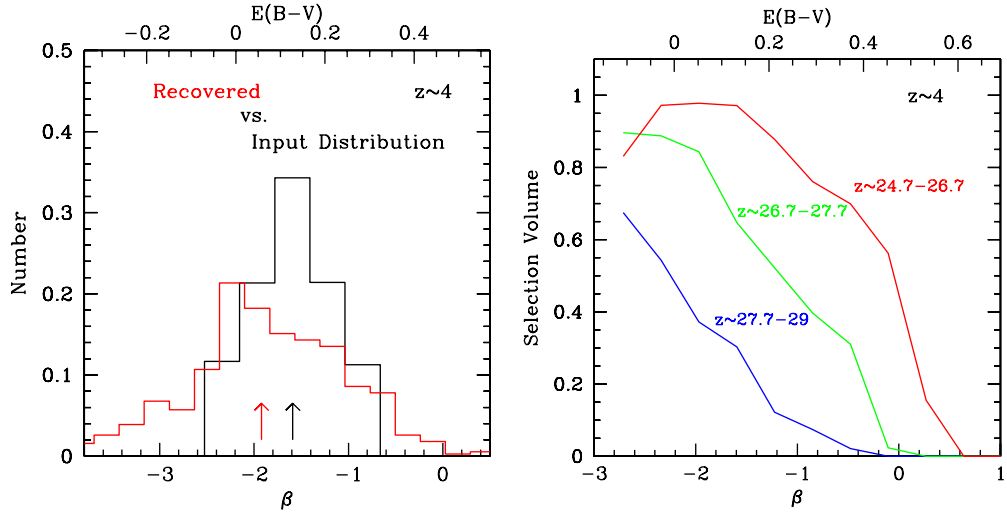

Figure 4. Left: comparison between the UV-continuum slope β distribution input into the simulations (black histogram) and that directly recovered from the simulations (red histogram; which included the effect of object selection and measurement error). This panel is for our faintest, lowest S/N $z \sim 4$ B-dropout selection over the HUDF (z_{850}-band magnitudes of 28–29). Both the input (and recovered) distributions are normalized to have the same area. On the top axes are the $E(B-V)$ extinctions (Calzetti et al. 2000 law) that are equivalent to a given β if the base spectrum is a young star-forming galaxy (∼100 Myr of constant star formation). The median UV-continuum slope β input into the simulations and that recovered are shown with the black and red arrows, respectively. The recovered distribution of UV-continuum slopes is broader and peaked to somewhat bluer values than the input distribution. For our higher S/N selections, the differences between the input and recovered distributions are much smaller (the offsets between the red and blue squares in Figure 3 show the size of the corrections). For our faintest selections (as shown here) the differences can be larger. It is nonetheless reassuring that when these corrections are applied there is agreement between the mean UV-continuum slopes estimated in our shallower selections (where the corrections are larger) and in our deeper selections (where the corrections are smaller). For example, the mean UV-continuum slope derived at $z_{850,AB}$ ∼26.5–27 for our GOODS B-dropout selections (i.e., -1.81 ± 0.04 at -19.2 AB mag) agrees very well with that derived from our much higher S/N HUDF selections for the GOODS fields (i.e., -1.73 ± 0.07 for the HUDF). (right) The selection volumes (arbitrary units) available to galaxies for our B-dropout selection over the HUDF vs. UV-continuum slope β. Shown are the relative selection volumes for galaxies with z_{850} ∼24.7–26.7 (red line), z_{850} ∼26.7–27.7 (green line), and z_{850} ∼27.7–29.0 (blue line). We emphasize that the same normalization for the selection volume is used for all the three magnitude selections, demonstrating that it is much easier to select galaxies with red UV-continuum slopes at bright magnitudes than it is at faint magnitudes. The reason bright $z \sim 4$ galaxies are easier to select is that one needs to confirm that a source has a large Lyman break at $>1\sigma$, and this is easier to do at bright magnitudes. Selection biases and measurement errors are less for brighter samples (where the S/N is higher) and greater for fainter samples. The two panels here demonstrate how important it is for us to correct for selection biases and measurement uncertainties as we do in Section 3.7.

do not include the UV-continuum slope results for sources where the model magnification factors are substantially greater than 10—due to sizeable model-dependent uncertainties in the actual magnification and hence their luminosities (the uncertainties in the magnification factor for sources with such high-predicted magnifications can be very large, i.e., greater than factors of ∼3-4; see Appendix A of R. J. Bouwens et al. 2009, in preparation). Even for sources where the predicted magnification factors are smaller, the model magnification factors (and hence the luminosities corrected for lensing) are likely uncertain at the factor of ∼2 level (R.J. Bouwens et al. 2009, in preparation).

We include the UV-continuum slope determinations of these galaxies with those estimated from our field samples in Figure 3 (black points on the $z \sim 4$ panel). As a result of a substantial magnification from gravitational lensing (typical factors of ∼5–10), the intrinsic luminosities of galaxies found behind clusters are much lower on average than those found in our field samples. In general, we observe good agreement between the distribution of UV-continuum slopes β derived from our field samples and those inferred from our selections around clusters.

3.7. Selection Biases and Measurement Uncertainties

The distribution of UV-continuum slopes that we derive is quite clearly affected by the manner in which sources are selected. This is because dropout criteria include galaxies with bluer UV-continuum slopes more efficiently (i.e., over a larger range in redshift) than they do for galaxies with other colors. This is because it is much easier to identify a sharp break in the SED of a blue galaxy than it is for a galaxy that is somewhat redder. For galaxies with red enough colors (i.e., UV-continuum slopes β larger than 0.5), it is essentially impossible to robustly select a high-redshift galaxy using the dropout criteria, and in fact the only sources that would satisfy the selection criteria would do so because of photometric scatter. This is illustrated in Figures 2 and 4.

To control for this effect, we construct models of the UV-continuum slope β distribution, use these models to add artificial galaxies to real data, select sources from these data, and measure their UV-continuum slopes in the same way as from the real data. The goal is to construct a model that when "observed" reproduces the distribution of UV-continuum slopes β measured from the data. For the sizes and morphologies of the model galaxies used in the simulations, we start with the pixel-by-pixel profiles of the $z \sim 4$ B-dropout sample from the HUDF (Bouwens et al. 2007) and scale their sizes as $(1+z)^{-1}$ (for fixed luminosity) to match the observed size-redshift trends (Bouwens et al. 2006; see also Ferguson et al. 2004 and Bouwens et al. 2004). We use our well-tested "cloning" software (Bouwens et al. 1998a, 1998b, 2003, 2006, 2007) to perform these simulations. For the model UV LF at $z \sim 2$–6, we adopt the Schechter parameterizations determined by Reddy & Steidel (2009) at $z \sim 2.5$ and by Bouwens et al. (2007) at $z \sim 4$–6.

In performing these simulations, we account for the modest correlation between the UV-continuum slopes β of galaxies and their surface brightnesses. We determined the approximation correlation by examining 192 luminous (∼1–2 L^*_{UV}) galaxies in our GOODS B-dropout selection and comparing their observed β's with their sizes (half-light radii). Any correlation is potentially important, since it could substantially lower the efficiency with which we can select galaxies with very red UV-

continuum slopes β (e.g., Figure 4). We find that sources with $\beta \gtrsim -1$ are ~15% larger than galaxies with $-2 \lesssim \beta \lesssim -1$ and ~40% larger than galaxies $\beta \lesssim -2$—though there is significant object-to-object scatter (the correlation coefficient between size (half-light radius) and β is just ~0.3). Fortunately, this correlation seems to only have a modest effect on these selection volumes, decreasing it by only ~10% for the red galaxies and increasing it by only ~10% for the blue galaxies.

We experimented with a range of model UV-continuum slope β distributions to determine the effect of object selection and photometric scatter on the observed distribution of UV-continuum slopes β. These experiments were performed as a function of magnitude and the input color distribution (with mean UV-continuum slopes ranging from -1.5 and -2.2 and the input color distribution taken to be Gaussian). In general, we found that the recovered distribution of UV-continuum slopes β (after selection) is *bluer* than the input distributions (by $\Delta\beta \sim 0.1$) at lower luminosities for all of our dropout samples. As expected, we found that noise in the observations broadened the distribution of UV-continuum slopes β somewhat over that present in the input distribution. Figure 4 illustrates how observational selection and noise modifies the input distribution of slopes for a *B*-dropout selection over the HUDF.

We used the simulations described above to quantify changes in this distribution as simple shifts in the mean UV-continuum slope and 1σ scatter. We used the estimated shifts to correct the observed distribution of UV-continuum slopes β for these effects. This corrected distribution of UV-continuum slopes is plotted in Figure 3 as open red squares, with the 1σ scatter shown with the red error bars.

To verify that the corrections we apply in this section are accurate, we compared the mean UV-continuum slope β we estimate near the faint end ($z_{850,AB}$ ~26.5-27) of our shallower GOODS *B*-dropout selections (after correction) with those derived from our much higher S/N HUDF *B*-dropout selections in the same magnitude range. We find that they are in excellent agreement, i.e., -1.81 ± 0.04 at -19.2 AB mag for the GOODS fields versus -1.73 ± 0.07 for the HUDF. This suggests that the corrections we apply in this section are reasonably accurate ($\Delta\beta \lesssim 0.1$).

3.8. Uncertainties and Model Dependences

Before presenting the distribution of UV-continuum slopes β derived for each of the dropout selections, it is worthwhile to ask ourselves how our determinations may be affected by specific assumptions we make. We have already discussed the effect that errors in our photometry (and zero points) would have on the UV-continuum slope determinations (Section 3.3). A ~0.05 mag error in the derived colors would result in a ~0.15 change in the derived UV-continuum slope β. In an attempt to minimize such errors, we have exercised great care in obtaining a consistent set of colors across the optical and near-IR passbands for which we have data.

We would expect a similar error in the UV-continuum slope β from the fiducial SEDs we use to convert from the observed colors to UV-continuum slope β. The uncertainties on the derived slope from this conversion are $\lesssim$0.1 for our $z \sim 2.5$, $z \sim 5$, and $z \sim 6$ and $\lesssim$0.2 for our $z \sim 4$ sample (see the Appendix).

The UV-continuum slopes we derive for our selections also show some dependence upon the model redshift distributions. As discussed in the Appendix, small differences ($\Delta z \sim 0.1$) between the mean redshifts of dropout galaxies in our models and that present in reality have a small effect on the derived UV-continuum slopes β. Errors of $\Delta z \sim 0.1$ in the mean redshifts of these selections shift the derived β's by 0.02, 0.02, 0.01, and 0.05 for our $z \sim 2.5\,U$, $z \sim 4\,B$, $z \sim 5\,V$, and $z \sim 6\,i$ dropout selections, respectively. These are much smaller uncertainties than the $\Delta\beta \sim 0.15$ errors that would result from small systematics in the photometry (or uncertainties in the conversion from observed colors to UV-continuum slopes).

Similarly, the presence or absence of Lyα emission (at 1216 Å) in the spectra of sources in our selections is not expected to have a large effect on the measured UV-continuum slopes β themselves. This is because the measurements are made in passbands which are only sensitive to light redward of 1216 Å. The only exception to this is for our $z \sim 6\,i$-dropout selection, but even there for typical Lyα equivalent widths (EWs; ~50 Å rest frame; Dow-Hygelund et al. 2007; Vanzella et al. 2006, 2009; Stanway et al. 2007), the $J_{110} - H_{160}$ colors would only change by ~0.07—which would make the derived β's ~0.17 bluer. Nonetheless, the amount of flux in Lyα has an effect on the redshift distribution of the sources selected with our dropout criteria. For galaxies with Lyα EWs toward the upper end of the observed range (~50 Å rest frame; Shapley et al. 2003; Dow-Hygelund et al. 2007; Vanzella et al. 2006, 2009; Stanway et al. 2007), the mean redshift of our dropout selections increases by $\Delta z \sim 0.3$. This changes the derived β's by 0.06, 0.06, 0.03, and 0.15, respectively, for our four selections (the Appendix). However, since only a small fraction ($\lesssim$ 50%) of the star-forming galaxies at $z \sim$ 2–6 appear to show Lyα emission at these levels (Shapley et al. 2003; Dow-Hygelund et al. 2007; Vanzella et al. 2006; Stanway et al. 2007), the effect of the quoted uncertainties on β is likely much smaller than this (i.e., $\lesssim$0.075). Again, this is much smaller than the errors we would expect to result from small systematics in the photometry (or conversions to UV-continuum slopes β).

Lastly, one might ask whether interstellar absorption features may have an effect on the UV-continuum slopes β estimated from the broadband photometry. Fortunately, these absorption lines appear not to have a big effect on the measured slopes (i.e., $\Delta\beta \lesssim 0.1$) as demonstrated by Meurer et al. (1999; see Section 3.4 and Figure 3 from Meurer et al. 1999) given the wide wavelength range of the broadband filters used to estimate the slopes and the fact that most of these absorption lines occur at $\lesssim$1700 Å.

3.9. Results

In Table 4, we present the mean UV-continuum slopes and 1σ scatter observed for our four dropout samples after correction for selection effects and photometric scatter. This distribution is the same as that presented in Figure 3). We assume a minimum systematic error in the mean UV-continuum slope β of 0.15 as a result of possible (~ 0.05 mag) systematics in the measured colors (see Section 3.3) and small model dependencies in the conversion from the observed colors to UV-continuum slope β (see the Appendix).

There are clear trends that seem to be present in the distributions of UV-continuum slopes β as a function of redshift and UV luminosity. The first trend is a correlation between the mean UV-continuum slope and UV luminosity, in the sense that galaxies become bluer at lower UV luminosities. This trend is particularly significant for our $z \sim 2.5\,U$-dropout and $z \sim 4\,B$-dropout selections, and fitting the mean β versus UV luminosity to a line, we find $\beta = (-0.20 \pm 0.04)(M_{UV,AB} + 21) - (1.40 \pm 0.07 \pm 0.15)$ for our $z \sim 2.5\,U$-dropout sample and

Table 4
The Mean UV-Continuum Slope β and 1σ Scatter of Galaxies, as a Function of UV Luminosity[a,b]

$\langle M_{UV,AB} \rangle$	UV-Continuum Slope β	
	Mean[c]	1σ Scatter[d]
	$z \sim 2.5$ U-dropouts	
−21.73	$-1.18 \pm 0.17 \pm 0.15$	0.32
−20.73	$-1.58 \pm 0.10 \pm 0.15$	0.27
−19.73	$-1.54 \pm 0.06 \pm 0.15$	0.34
−18.73	$-1.88 \pm 0.05 \pm 0.15$	0.36
	$z \sim 4$ B-dropouts	
−22.22	$-1.32 \pm 0.12 \pm 0.15$	0.51
−21.72	$-1.33 \pm 0.07 \pm 0.15$	0.31
−21.22	$-1.44 \pm 0.04 \pm 0.15$	0.44
−20.72	$-1.51 \pm 0.03 \pm 0.15$	0.40
−20.22	$-1.58 \pm 0.10 \pm 0.15$	0.34
−19.72	$-1.68 \pm 0.09 \pm 0.15$	0.35
−19.22	$-1.73 \pm 0.07 \pm 0.15$	0.55
−18.72	$-1.93 \pm 0.06 \pm 0.15$	0.31
−18.22	$-1.98 \pm 0.05 \pm 0.15$	0.54[e]
−17.72	$-2.03 \pm 0.04 \pm 0.15$	0.29[e]
−17.22	$-1.91 \pm 0.05 \pm 0.15$	0.26[e]
	$z \sim 5$ V-dropouts	
−21.90	$-1.81 \pm 0.22 \pm 0.15$	0.45
−20.90	$-1.76 \pm 0.10 \pm 0.15$	0.64
−19.90	$-2.17 \pm 0.08 \pm 0.15$	0.66[e]
−18.90	$-2.64 \pm 0.16 \pm 0.15$	1.02[e]
	$z \sim 6$ i-dropouts	
−20.76	$-2.16 \pm 0.15 \pm 0.15$	0.41
−18.76	$-2.32 \pm 0.19 \pm 0.15$	0.91[e]

Notes.
[a] The mean UV-continuum slopes β (1600–2300 Å) presented here are also shown on Figure 3 as the red squares.
[b] The slopes presented here have been corrected for selection effects and measurement errors (see Section 3.7). The tabulated UV luminosities are the geometric mean of the UV luminosity measured in the two bands used to establish the UV slope (see Table 2).
[c] Both random and systematic errors are quoted (presented first and second, respectively). In Section 3.8, we estimate the likely size of the systematic errors.
[d] The 1σ scatter presented here has been corrected for photometric scatter using the simulations described in Section 3.7 (see also Figure 4) and therefore should reflect the intrinsic 1σ scatter in the UV-continuum slope β distribution. Typical uncertainties are ∼0.05–0.10.
[e] Because the observed scatter in the UV-continuum slopes for the faintest sources is dominated by the photometric errors, it is very difficult to estimate the intrinsic 1σ scatter in the β distribution, and therefore the uncertainties on our estimates of the intrinsic scatter in the β distribution are large, i.e., $\gtrsim$0.2–0.4.

$\beta = (-0.15 \pm 0.01)(M_{UV,AB} + 21) - (1.48 \pm 0.02 \pm 0.15)$ for our $z \sim 4$ B-dropout sample (the fit is shown in Figure 3 with the red lines).[9] The $\Delta\beta$ errors of ± 0.15 given in the equations above are our estimates of the systematic errors (see discussion in the previous section). We find no significant trend in the width of the UV-continuum slope β distribution as a function of luminosity.

[9] While we find a strong correlation between the UV-continuum slope β and the observed UV magnitude at $z \sim 2.5$ over the range $V_{606,AB} \sim 23$–27, it appears that the UV-continuum slope β shows a weaker dependence on magnitude at brighter magnitudes, i.e., $V_{606,AB} \sim$ 23-25.5. Adelberger & Steidel (2000) and Reddy et al. (2008) find no correlation between these quantities over this magnitude range, and a t-test applied to our $z \sim 2.5$ U-dropout sample shows a correlation at only 75% confidence over this magnitude range.

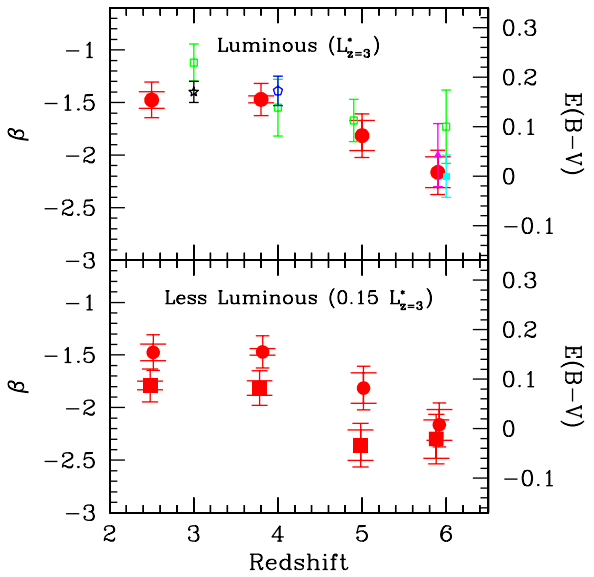

Figure 5. Top: determinations of the mean UV-continuum slope β for galaxies with a UV luminosity of $L^*_{z=3}$ ($M_{UV} \sim -21$) as a function of redshift (solid red circles). The error bars in β are $\geqslant 0.15$ and include possible systematic errors in both the measured colors and corrections for selection effects. The error bars in β (with the wider horizontal bars) are for the random errors. The random errors are generally much smaller than those including the estimated systematic errors (shown with the narrower horizontal bars). The right axes give the equivalent $E(B-V)$ extinctions (Calzetti et al. 2000 law) for a given β if the input spectrum is a young star-forming galaxy (∼100 Myr of constant star formation). Published determinations of the mean UV-continuum slope β at $z \sim 3$ (black star; Adelberger & Steidel 2000), at $z \sim 4$ (blue open pentagon; Ouchi et al. 2004), at $z \sim 6$ (solid cyan square; Stanway et al. 2005 and solid magenta triangle; Bouwens et al. 2006), and at $z \sim$4–6 (green open squares; Hathi et al. 2008) are also plotted. $L^*_{z=3}$ galaxies are found to have bluer colors at $z \sim$ 5–6 than they do at $z \sim$ 2–4. Bottom: determinations of the mean UV-continuum slope β for galaxies with a UV luminosity of $0.15L^*_{z=3}$ ($M_{UV} \sim -19$) as a function of redshift (solid red squares). For comparison, our determinations of the mean UV-continuum slope β at $L^*_{z=3}$ (from top panel) are included in this panel as solid red circles (and offset somewhat from the lower luminosity determinations in redshift for clarity). For each of our dropout samples, the lower luminosity galaxies are found to be bluer.

We also find a clear correlation between the mean UV-continuum slope β and redshift, in the sense that higher redshift galaxies are bluer. This is most evident in Figure 5 where the mean UV-continuum slope β is shown at a luminosity of $L^*_{z=3}$ (i.e., $M^*_{UV} \sim -21$) and $0.15L^*_{z=3}$ (i.e., $M^*_{UV} \sim -19$) for each of our dropout samples. At $z \sim$ 2–4, the mean UV-continuum slope is ~ -1.5 while at $z \gtrsim 5$, it is $\lesssim -1.8$. No change is evident in the width of the UV-continuum slope distribution—though this width is difficult to quantify for our highest redshift samples due to the small number of sources in these high-redshift samples and the large photometric errors of the sources that are available.

4. THE UV-CONTINUUM SLOPE DISTRIBUTION: DIRECT IMPLICATIONS

In Section 3, the UV-continuum slope β distribution was derived as a function of both redshift and luminosity. Being able to establish this distribution as a function of these two quantities is an important empirical result and has a number of noteworthy implications, which we will detail in this section. However, before describing these implications, it is prudent to compare the present UV-continuum slope β determinations with those in the literature to put them in context (see Section 4.1).

One of the most significant implications of these results is for the completeness of dropout selections at $z \sim$2–6, which we discuss in Section 4.2. Being able to establish these distributions

is also important for a determination of the $z \sim$ 2–6 LFs (Section 4.3). In Section 4.4, we consider the question of how variations in the UV-continuum slope β likely arise, and we argue that changes in the dust extinction likely dominate the observed variations. Finally, in Section 4.5, we attempt to connect the sequence we find in the UV-continuum slope versus luminosity to similar trends found at lower redshift (and over other wavelength baselines).

4.1. Comparison to Previous Determinations of the UV-Continuum Slope

In Section 3, we derived the distribution of UV-continuum slopes β over a wide range in redshift and UV luminosity using a very systematic approach while taking advantage of a wide variety of both deep and wide-area *HST* data. We presented evidence that the mean UV-continuum slope β is bluer at $z \sim$ 5–6 than it is at $z \sim$ 2–4 and that this slope is also bluer at lower UV luminosities at $z \sim$ 2–4.

Previously, there had been a variety of different attempts to measure these slopes at specific redshifts or luminosities (typically $\sim L^*_{z=3}$), e.g., Steidel et al. (1999), Meurer et al. (1999), Adelberger & Steidel (2000), Ouchi et al. (2004), Stanway et al. (2005), Bouwens et al. (2006), and Hathi et al. (2008). The top panel of Figure 5 provides a summary of many of these previous measurements. Most of the early high-redshift work focused on $z \sim$ 2–3 and was based upon *U*-dropout selections from the HDF and large ground-based LBG searches (e.g., Steidel et al. 1999; Adelberger & Steidel 2000; Meurer et al. 1999). In these papers, the UV-continuum slope β was found to have a mean value of ~ -1.4 and 1σ dispersion of $\sim$0.5–0.6 at $\sim L^*_{UV}$. No significant correlation of UV-continuum slope β with UV magnitude was found to -20 AB mag (Adelberger & Steidel 2000; Reddy et al. 2008), though there would appear to be some evidence in the β distributions presented by Meurer et al. (1999, e.g., Figure 5 from that paper) that the β distribution becomes a little bluer at lower UV luminosities (i.e., -18.5 AB mag).[10]

Ouchi et al. (2004) extended these studies to higher redshift by presenting a determination of the UV-continuum slope distribution at $z \sim 4$ based on a large selection of *B*-dropout galaxies from the Subaru Deep Field and Subaru *XMM/Newton* Deep Field. Ouchi et al. (2004) found that the UV-continuum slope distribution at $z \sim 4$ was consistent with that determined at $z \sim 3$ and that there was only a marginal trend (not statistically significant) toward bluer slopes at lower luminosities. Papovich et al. (2004), by contrast, working with a selection of $z \sim 4$ *B*-dropouts from the GOODS fields, found that galaxies at $z \sim 4$ were slightly bluer in their UV colors than at $z \sim 2.5$ in the HDF North and South. At somewhat fainter magnitudes, Beckwith et al. (2006) remarked that the UV colors of $z \sim 4$ *B*-dropouts in the HUDF were very blue in general (with β's of ~ -2) and hence suggested very little dust extinction. The somewhat bluer UV-continuum slopes found by Beckwith et al. (2006) than by, e.g., Ouchi et al. (2004) is not particularly surprising given the substantial differences in the mean luminosities of the two samples. Incidentally, the trend toward bluer UV-continuum slopes at lower luminosities reported on here is evident in Figure 18 of Beckwith et al. (2006) although it was not specifically noted.

[10] Unfortunately, Meurer et al. (1999) do not provide a lot of discussion on the possible correlation of β with observed UV luminosity (despite the existence of a likely trend) and instead emphasizes the correlation of β with *dust-corrected* UV luminosity.

At even higher redshifts, Lehnert & Bremer (2003) found that $z \sim 5$ *V* dropouts had UV-continuum slopes β very close to -2 while later Stanway et al. (2005) and Bouwens et al. (2006) found UV-continuum slopes of -2.2 ± 0.2 and -2.0 ± 0.3, respectively, at $z \sim 6$ from a selection of *i*-dropouts in the HUDF. Hathi et al. (2008) used a small sample of galaxies at $z \sim$4–6 from the HUDF and larger sample of *U*-dropouts at $z \sim 3$ in an attempt to quantify the change in the UV-continuum slope β as a function of redshift. Hathi et al. (2008) found that the UV-continuum slope β showed only a slight change from $z \sim 3$ (where $\beta \sim -1.5$) to $z \sim$ 5–6 (where $\beta \sim -1.8$).

Broadly, the picture that has emerged from these studies is that star-forming galaxies become bluer toward higher redshifts and to lower luminosities, but it has been difficult, given possible systematics between the different studies, to quantify the size of the changes. We confirm this overall picture, finding that the mean UV-continuum slope is $\sim 1.0 \pm 0.4$ bluer at $z \sim 6$ than it is at $z \sim 2.5$ and $\sim 0.5 \pm 0.1$ bluer at -18 AB mag ($\sim 0.1 L^*_{z=3}$) than it is at -21 AB mag ($\sim L^*_{z=3}$). Because of the larger samples and use of a consistent approach in deriving these slopes at all redshifts and luminosities, the differential evolution we measure is more robust than in previous studies.

Looking more specifically at the UV-continuum slope β measurements we have derived at various redshifts and comparing those measurements with those obtained in previous studies, we find very good agreement in general, in almost all cases within the quoted errors. The only significant exception to this is the Hathi et al. (2008) measurements of the UV-continuum slope β at $z \sim 6$ where a mean β of -1.73 ± 0.35 was found. This appears to result from the relation Hathi et al. (2008) use to compute the UV-continuum slope β at $z \sim 6$ (i.e., $\beta = 2.56(J - H) - 2$). This relation does not account for the fact that the NICMOS J_{110} band extends down to 8000 Å and therefore $z \sim 6$ *i*-dropouts partially drop out in the J_{110} band (i.e., are fainter in the J_{110} band and hence have redder $J_{110} - H_{160}$ colors). Comparing $\beta = 2.56(J - H) - 2$ with Equation (A5) from the Appendix, we can readily see why the mean UV-continuum slopes we derive are much steeper (by $\sim$0.3). We note that an additional -0.1 mag shift in β relative to previous $z \sim 6$ measurements of β (e.g., Bouwens et al. 2006; Hathi et al. 2008) comes from small offsets we make to the J_{110}-band photometry (Section 3.3).

4.2. Do LBG Selections Miss a Substantial Population of Red Star-forming Galaxies at $z \gtrsim 4$?

The LBG selection technique identifies galaxies at high redshift through simple color criteria. This technique is well established to be an efficient and robust method for identifying star-forming galaxies over a wide range in redshift $z \sim$ 2–6 (Steidel et al. 1996; Williams et al. 1996; Bunker et al. 2003; Vanzella et al. 2006, 2009; Dow-Hygelund et al. 2007). This technique provides a very complete census of UV light at high redshift—simply by virtue of the selection wavelength itself. However, it is less efficient for probing the total stellar mass or even the total SFR at high redshift (e.g., van Dokkum et al. 2006). This is because galaxies with the highest stellar masses or SFRs are often either old or dust obscured—making them fainter in the UV and thus more difficult to select with the LBG technique.

Our interest here is in examining the systemic completeness of LBG selections. We want to determine whether there is a set of galaxies at high redshift that we miss altogether by virtue of the LBG selection technique. Note that this is a very different

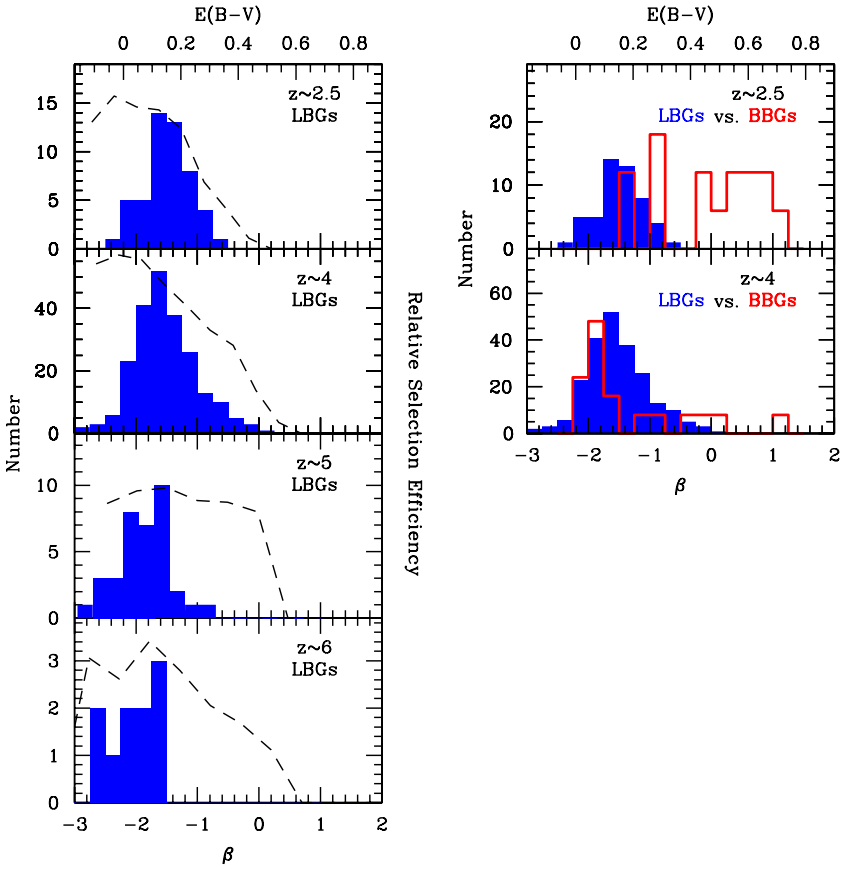

Figure 6. Left: distribution of UV-continuum slopes β observed at $z \sim 2$–6 for the present LBG selections (solid blue histograms). We only include the observed β values for LBGs >1 mag brighter than the selection limit to avoid being dominated by selection effects. On the top axes are the $E(B-V)$ extinctions (Calzetti et al. 2000 law) that are equivalent to a given β if the base spectrum is a young star-forming galaxy ($\sim$ 100 Myr of constant star formation). The selection volume (Section 3.7) available for galaxies with UV-continuum slope β and magnitudes $\gtrsim$ 1 mag brighter than the selection limit is shown with the thick dashed lines in each panel (the normalization is arbitrary). While it is more difficult to select galaxies with redder UV-continuum slopes β with a Lyman break criterion, our simulations (Section 3.7) indicate that our dropout selections should be capable of identifying modest numbers of galaxies with β's as red as 0.5. Indeed, such galaxies (with β's redder than -1) are present in our $z \sim 2$–4 LBG selections albeit in small numbers. However, they are conspicuously absent in our $z \gtrsim 5$ selections. This suggests that such sources are exceedingly rare at $z \gtrsim 5$. Conversely, the modest number of galaxies with red UV-continuum slopes β's seen at $z \sim 4$ seem consistent with the small samples of $z \sim 4$ ULIRGs that have been found in the observations (e.g., Daddi et al. 2009). The lack of very blue $\beta \lesssim -3$ galaxies is also consistent with expectations from models and suggest that the β distributions derived here are reliable. Right: distribution of UV-continuum slopes observed for LBG selections at $z \sim 2$–4 (solid blue histogram) and for BBG selections at $z \sim 2$–4 (red histogram; Brammer & van Dokkum 2007). The $E(B-V)$ extinctions given on the top axis are as in the left panel (but are not expected to be particularly representative for the somewhat older BBGs). Both β distributions plotted are as observed, with no correction for selection or measurement effects. BBG selections provide us with an independent measure of the UV-continuum slope distribution since they do not depend upon their UV-continuum slope or the brightness of these sources in the UV-continuum. The fact that the distribution of UV-continuum slopes β is becoming substantially bluer for both selections (and in particular the Brammer & van Dokkum 2007 BBG selection at $z \sim 4$) suggests that Lyman-break selections (sensitive to galaxies with β's bluer than 0.5: see Figures 2 and 4) should be largely complete at $z \gtrsim 5$ (see Section 4.2).

question from determining whether there is a class of galaxy at high redshift that we select *less efficiently* because they are faint in the UV (e.g., because of dust or age). In general, we would expect sources to miss our LBG selections if one of the two LBG color criteria failed to hold, i.e., if (1) the sources did not show a strong Lyman break or (2) the sources were too red in their UV-continuum slope to satisfy the LBG selection. We would expect criterion (1) to always hold for a sufficiently high redshift source, as a result of line blanketing by the Lyα forest. However, we might expect criterion (2) to fail if the UV-continuum slopes β of the sources were sufficiently red.

We can attempt to address this question by looking at how many galaxies have UV-continuum slopes β that lie close to the selection limits. If our samples contain a large number of such galaxies, it would suggest that our LBG selections suffer from significant incompleteness near these limits. Figure 2 shows the selection criteria for each of LBG selections and Figure 6 presents the effective search volume (Section 3.7) for galaxies (dashed black lines on the left-hand panels) as a function of UV-continuum slope β (see also Figure 4). It is quite clear from these figures that our selection criteria are effective in identifying star-forming galaxies at $z \sim 2$–6 with β's bluer than $\sim$0.5, and it is striking how much redder this limit is than the UV-continuum slopes derived for galaxies in our dropout samples at $z \sim 2$–6 (solid blue histograms in Figure 6). The situation is particularly conspicuous for galaxies with UV-continuum slopes β redder than -1 at $z \gtrsim 5$. While our simulations (Section 3.7) suggest that galaxies with these colors should show up in our selections if they existed (dashed lines in Figure 6), essentially none are found. This suggests that star-forming galaxies with red UV-continuum slopes β are extremely rare.

Complementary Balmer Break Selections. Another way we can investigate the issue of possible systemic incompleteness in LBG selections is through other selection techniques. One such technique identifies galaxies based upon their rest-frame optical light and searches for a prominent Balmer break at $\sim$3700 Å

rest frame. Such selections are not surprisingly called Balmer Break Galaxy (BBG) selections and typically identify the oldest and most massive galaxies. Since such galaxies tend to be more chemically evolved, they are frequently dustier. Considering such selections therefore permit us to evaluate the extent to which our LBG selections may miss redder and more dust-obscured starbursts. Brammer & van Dokkum (2007) performed such a selection at $2 < z < 3$ and $3 < z < 4.5$ (see right-hand panels in Figure 6) based upon the Faint Infrared Extragalactic Survey (FIRES) data (Labbé et al. 2003; Förster Schreiber et al. 2006) and derived UV-continuum slopes for sources in their selections from SED fits to the photometry. They found that ∼67% of the galaxies in their $z \sim$ 2–3 selection had UV-continuum slopes bluer than 0.5, but almost all ($\gtrsim$ 90%) of the galaxies in their $z \sim$3–4.5 sample had such blue slopes. This is highly encouraging for $z \sim 4$ LBG selections given the independent nature of Balmer Break selections—suggesting that $z \sim 4$ LBG selections may be largely complete.

By contrast, the fact that ∼33% of the galaxies in the Brammer & van Dokkum (2007) $z \sim$ 2–3 BBG sample have β's redder than 0.5 suggests that completeness could be somewhat of a concern for LBG selections at $z \sim 2.5$, and in fact it is well known that at $z \sim$ 2–3, there is a substantial population of dust-obscured galaxies undergoing vigorous star formation (e.g., Hughes et al. 1998; Barger et al. 1998; Chapman et al. 2005; Labbé et al. 2005; Papovich et al. 2006; Pope et al. 2006).

Searches for BBGs at $z \gtrsim 5$ have also been conducted (e.g., Dunlop et al. 2007; Wiklind et al. 2008; see also Rodighiero et al. 2007 and Mancini et al. 2009). As with the Brammer & van Dokkum (2007) study, these searches would seem to be relevant to the present discussion we are having about the completeness of LBG selections for star-forming galaxies at high redshift. Unfortunately, there is a wide diversity of search results in this area that make it difficult to draw clear conclusions. Wiklind et al. (2008) report 11 plausible BBGs at $z \sim$ 5–7 over the Chandra Deep Field-South GOODS field, 7 of which are detected at 24 μm with MIPS, while Dunlop et al. (2007) find no BBGs over the same redshift range, in their analysis of the same field. While the MIPS detections for 7 of the 11 $z \sim$ 5–7 Wiklind et al. (2008) BBG candidates may be interpreted as due to an obscured active galactic nucleus (AGN), we believe that a much more likely explanation is due to PAH emission, as Chary et al. (2007b) argue for HUDF-JD2 (Mobasher et al. 2005). The other BBG candidates from Wiklind et al. (2008) may have redshifts of $z \sim$ 5–7, but may also have lower redshifts.

Implications. Putting together the present LBG selection results at $z \sim$ 2–6 with those from Balmer break selections over the same range and other results in the literature, we find clear evidence that the galaxy population at high redshift is increasingly blue as one moves out to high redshift, and therefore high-redshift LBG selections seem likely to be increasingly complete (and consequently suffer much less from systematic incompleteness). These trends are very clear in LBG selections at $z \sim$ 2–6, and since there is no reason to suppose that these trends come from various selection biases (not only do the sources have β's very far from the selection limits, but the effect of observational selection are corrected for), it seems reasonable to take the observed evolution at face value. Supporting evidence comes from a similar evolution seen in complementary Balmer break selections (at least according to Brammer & van Dokkum 2007). Previously, Bouwens et al. (2007; Section 4.1) have discussed this in the context of $z \sim 4$ B-dropout selections.

Table 5
The Effective Dust Extinction (at ∼1600 Å) Estimated for the LBG Population Integrated Down to Various UV Luminosities (see also Figure 8)

Sample	Effective Extinction		
	$> 0.3L^*_{z=3}$	$> 0.04L^*_{z=3}$	> 0
Using Meurer et al. (1999) Relationship[a,b]			
U-dropouts	$6.0^{+1.8+2.1c}_{-1.4-1.6}$	$3.8^{+0.8+1.4}_{-0.6-1.0}$	$2.8^{+0.5+1.0}_{-0.4-0.7}$
B-dropouts	$5.8^{+0.8+2.1}_{-0.7-1.5}$	$3.8^{+0.5+1.3}_{-0.5-1.0}$	$2.8^{+0.3+1.0}_{-0.3-0.7}$
V-dropouts	$2.7^{+0.7+1.0}_{-0.5-0.7}$	$1.6^{+0.3+0.6}_{-0.2-0.4}$	$1.4^{+0.2+0.5}_{-0.2-0.4}$
i-dropouts	$1.6^{+0.4+0.6}_{-0.3-0.4}$	$1.3^{+0.3+0.5}_{-0.3-0.4}$	$1.2^{+0.2+0.4}_{-0.2-0.3}$

Notes.
[a] The effective dust extinctions given here are the multiplicative factors needed to correct the observed UV luminosity densities at ∼1600 Å to their intrinsic values, after integrating to specific limiting luminosities (with the limits specified in the columns). These extinctions are estimated based upon the distribution of UV-continuum slopes observed (Table 4) and the correlation between UV-continuum slope and dust obscuration observed at $z \sim$ 0–2 (Equation (1); Meurer et al. 1999). Note that the dust extinctions are much lower when integrated to very low luminosities.
[b] Both random and systematic errors are quoted (presented first and second, respectively).
[c] This estimate is in good agreement with the estimates at $z \sim 2$ by Reddy et al. (2006) and Erb et al. (2006b) from various multiwavelength data, but 3 times larger than what Carilli et al. (2008) obtained stacking radio observations for $> 0.2L^*_{z=3}$ $z \sim 3$ U-dropouts in the COSMOS field (Section 5.4).

Obviously we would expect galaxies at very high redshifts ($z \sim$ 5–6) to have much bluer UV-continuum slopes than at $z \sim$2–3, because of the much smaller time baseline over which to produce metals and dust, as well as the shorter dynamical timescales of galaxies at $z \gtrsim 5$ (and hence much reduced ages). We would also expect this result based upon the evolution of the UV LF. Since the characteristic luminosity of galaxies in the UV becomes progressively smaller as we move to higher redshifts (Dickinson et al. 2004; Shimasaku et al. 2005; Bouwens et al. 2006, 2007; Yoshida et al. 2006; Oesch et al. 2009), we would expect to find fewer and fewer galaxies at high redshift with very large SFRs. Since dust extinction is well correlated with the SFR (e.g., Wang & Heckman 1996; Hopkins et al. 2001; Martin et al. 2005; Reddy et al. 2006; Buat et al. 2007; Zheng et al. 2007), we would not expect to find many galaxies at $z \gtrsim 5$ with substantial dust extinction. Finally there is the evolution seen in the relationship between SFR and dust extinction. From $z \sim 0$ to $z \sim 0.7$ to $z \sim 2$, it has been found that the effective dust extinction for a given SFR decreases quite strongly as we move out to higher redshifts (Reddy et al. 2006; Buat et al. 2007; Burgarella et al. 2007). Each of these considerations suggest that galaxies at high redshift should be almost uniformly very blue and LBG selections very complete.

Nonetheless, we know there is a substantial population of luminous, dust-obscured galaxies at $z \sim$2–3 (e.g., Hughes et al. 1998; Barger et al. 1998; Chapman et al. 2005; Labbé et al. 2005; Papovich et al. 2006; Pope et al. 2006) and extending out to redshifts as high as $z \sim 4.5$ (e.g., Capak et al. 2008; Daddi et al. 2009; Wang et al. 2009; Dannerbauer et al. 2008). While some authors (e.g., Daddi et al. 2009) make the suggestion that these populations might be quite significant and contribute substantially to the overall SFR density at $z \gtrsim 4$, we would argue that the role of these galaxies is likely much more modest in scope and they do not provide a large fraction of the SFR density, particularly at $z \gtrsim 4$. We discuss and quantify this point in Section 6.2 (see also Tables 5, 7, and Figures 13 and 14).

Table 6
Inferred Star Formation Rate Densities from $z \sim 2$–6 LBG Samples[a,b]

Dropout Sample	$\langle z \rangle$	$\log_{10}$ SFR density ($M_\odot$ Mpc^{-3} yr^{-1}) $L > 0.3L^*_{z=3}$	$L > 0.04L^*_{z=3}$
		Uncorrected	
U	2.5[c]	-1.70 ± 0.03	-1.36 ± 0.03
B	3.8	-1.81 ± 0.05	-1.48 ± 0.05
V	5.0	-2.15 ± 0.06	-1.78 ± 0.06
i	5.9	-2.31 ± 0.08	-1.83 ± 0.08
z	7.4	-2.58 ± 0.21	...
		Dust-Corrected	
U	2.5[c]	-0.93 ± 0.03	-0.78 ± 0.03
B	3.8	-1.05 ± 0.05	-0.90 ± 0.05
V	5.0	-1.72 ± 0.06	-1.57 ± 0.06
i	5.9	-2.10 ± 0.08	-1.70 ± 0.08
z	7.4	-2.37 ± 0.21	...

Notes.
[a] Based upon LF parameters in Table 2 of Reddy & Steidel (2009), Table 7 of Bouwens et al. (2007; see Section 3.5), and Table 4 of Bouwens et al. (2008).
[b] The SFR density here tabulated in terms of the Salpeter IMF. Expressing these results in terms of a Kroupa (2001) IMF, one should divide the results given here by a factor of ~1.7.
[c] We adopt the Reddy & Steidel (2009) UV LF at $z = 3$ for computing the SFR density at $z \sim 2.5$.

Table 7
Inferred Star Formation Rate Densities, Including the Contributions from Highly Dust Obscured Galaxies (Sections 6.2–6.3)[a,b]

Dropout Sample	$\langle z \rangle$	$\log_{10}$ SFR Density ($M_\odot$ Mpc^{-3} yr^{-1}) $L > 0.3L^*_{z=3}$	$L > 0.04L^*_{z=3}$
		Dust-Corrected	
U	2.5[c]	-0.93 ± 0.03	-0.78 ± 0.03
B	3.8	-1.05 ± 0.05	-0.90 ± 0.05
V	5.0	-1.72 ± 0.06	-1.57 ± 0.06
i	5.9	-2.10 ± 0.08	-1.70 ± 0.08
z	7.4	-2.37 ± 0.21	...
		Dust-Corrected + ULIRG[d]	
U	2.5[c]	-0.77 ± 0.03	-0.66 ± 0.03
B	3.8	-0.98 ± 0.05	-0.85 ± 0.05
V	5.0	-1.66 ± 0.06	-1.53 ± 0.06
i	5.9	-2.07 ± 0.08	-1.69 ± 0.08
z	7.4	-2.37 ± 0.21	...

Notes.
[a] Based upon LF parameters in Table 2 of Reddy & Steidel (2009), Table 7 of Bouwens et al. (2007; see Section 5.6), and Table 4 of Bouwens et al. (2008).
[b] The SFR density here tabulated in terms of the Salpeter IMF. Expressing these results in terms of a Kroupa (2001) IMF, one should divide the results given here by a factor of ~1.7.
[c] We adopt the Reddy & Steidel (2009) UV LF at $z = 3$ for computing the SFR density at $z \sim 2.5$.
[d] At $z \sim 2.5$, we include the SFR density contribution from $> 10^{12} L_\odot$ ultraluminous IR galaxies (ULIRGs; Section 6.2) by using the $z \sim 2$ IR LF of Caputi et al. (2007) as Reddy & Steidel (2009) do. At $z \sim 4$, we estimate their contribution based upon a small sample of $z \sim 4$ ULIRG candidates (see Daddi et al. 2009) within the HDF-North GOODS SCUBA supermap (Pope et al. 2006). Based upon the $z \sim 4$ result, we assume that ULIRGs provide only a ~5% contribution to the SFR density at $z \sim 5$–6. We believe that this assumption is a reasonable one given the trends toward much bluer UV-continuum slopes at high redshifts seen in both LBG and BBG samples (Section 4.2) and thus an apparently smaller fraction of galaxies with substantial dust obscuration.

4.3. Relevance for LF Determinations

As shown in Figures 2–6 (and as discussed in the previous section), the effective selection volume for star-forming galaxies at $z \sim 2$–6 is very sensitive to its UV-continuum slope β and UV luminosity and can vary by factors of $\gtrsim 2\times$ (see also discussion in Sawicki & Thompson 2006a or Beckwith et al. 2006). Quantifying the distribution of UV-continuum slopes for star-forming galaxies (as a function of both luminosity and redshift) is therefore an important first step in determining the UV LFs at high redshift.

Given this impact, it has been somewhat surprising that different teams have made very different assumptions about the distribution of UV-continuum slopes in their determinations of the UV LFs. Some teams have adopted UV-continuum slopes of $\beta \sim -1.4$ (Sawicki & Thompson 2006a; Yoshida et al. 2006), other teams have assumed UV-continuum slopes of $\beta \sim -2.0$ (Beckwith et al. 2006), and yet other teams have adopted luminosity-dependent UV-continuum slopes (Bouwens et al. 2007). Such differences have only added to the large dispersion seen in LF determinations at high redshift (see Figures 10, 11, and 13 from Bouwens et al. 2007).

As a result of the present quantification of UV-continuum slopes β at high redshift (versus redshift and luminosity), we now have a relatively uniform set of assumptions that can be used for quantifying the UV LFs at $z \sim 2$–6 and in extending such determinations to $z \gtrsim 7$.

4.4. Interpreting Variations in the UV-Continuum Slope β

Having used the available observations to derive the distribution of UV-continuum slopes β for high-redshift galaxies as a function of UV luminosity and a range in redshift (Table 4 and Figure 3), we might ask ourselves what this teaches us about the physical properties of high-redshift galaxies. Since the UV-continuum slope β is purely an observational measure of the shape of the spectrum of high-redshift galaxies and can be affected by a variety of different physical conditions (including dust, age, metallicity, etc.), we cannot use the above measurements to make any unambiguous observational inferences about the nature of high-redshift galaxies.

Nevertheless, we will argue that the simplest way to explain most of observed differences in β is through changes in the dust content of galaxies. While there are certainly variations in other quantities such as the age, metallicity, or IMF of the stars that affect these slopes, we will argue that variations in the dust content of galaxies likely have the largest effect on the observed UV-continuum slopes and we can use the observed variations in these slopes to make inferences about changes in the effective dust extinction as a function of galaxy luminosity and redshift.

We note that we would not expect the presence or luminosity of an AGN to have a big effect on these slopes, given that the observed incidence of such sources at $z \sim 2$–4 is just ~3% for moderately bright galaxies at $z \sim 2$–3 (e.g., Nandra et al. 2002) and there is little evidence they are more frequent or important at higher redshifts or lower luminosities (e.g., Lehmer et al. 2005; Ouchi et al. 2008).

To ascertain which of the aforementioned factors (e.g., the overall dust content and properties, the age, metallicity, or IMF of a stellar population) are likely to be the most important for interpreting the variations we see in the UV-continuum slopes β, we consider the effect that changes in many of the above quantities would have on the UV-continuum slope β. For simplicity, we model the star formation history of galaxies with a simple τ model $e^{-t/\tau}$ with $\tau = 10$ Myr (e.g., as in Papovich et al. 2001) and t equal to the age. We also take the metallicity

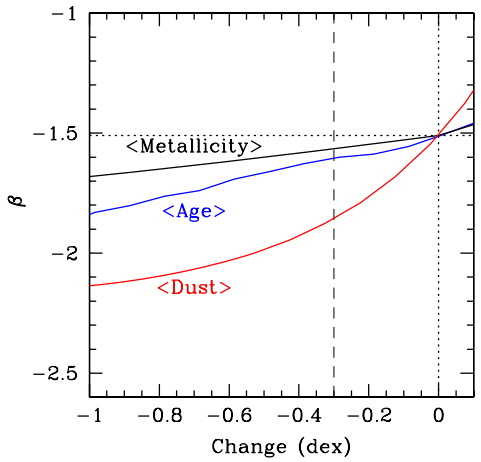

Figure 7. UV-continuum slope β (1600–2300 Å rest-frame baseline) predicted for specific fractional changes in the mean age, metallicity, or dust extinction of high-redshift star-forming galaxies from our fiducial stellar population model. For our fiducial model (where $\beta = -1.47$), we assume $t = 70$ Myr, $\tau = 10$ Myr, $[Z/Z_{\odot}] = -0.7$, $E(B-V) = 0.15$, and a Salpeter IMF (where the star formation history is parameterized as $e^{-t/\tau}$) from the Papovich et al. (2001) fits to $z \sim 2.5$ U-dropouts from the WFPC2 HDF North. In modifying our fiducial model to have younger ages, we make changes to both t and τ. A factor of 2 (0.3 dex) change (dashed line) in the mean dust content, age, or metallicity of the star-forming galaxy population at high-redshift shifts the UV-continuum slope β by ∼0.35, ∼0.1, and ∼0.05, respectively. The effect of the stellar IMF on β is not shown here, but results in only modest changes in β, i.e., $\Delta\beta \lesssim 0.1$ for a ∼0.5 shift in the slope of the IMF. It seems clear that changes in the mean dust content of galaxies at high redshift has the biggest effect on the UV-continuum slope β—though some change is also likely the result of differences in the average age. Nonetheless, since stellar population modeling of $z \sim 4$–6 dropout galaxies (Stark et al. 2009) suggest that age shows little dependence on redshift or luminosity (at least in the median), it seems likely that age only plays a minor role ($\Delta\beta \lesssim 0.2$) in driving the observed trends (Section 4.4).

to be fixed and not evolve over this entire history. Finally, we implement the dust extinction by applying the Calzetti et al. (2000) law to the SED resulting from the stellar population models (Bruzual & Charlot 2003). Using the Papovich et al. (2001) modeling of $z \sim 2.5U$-dropouts in the HDF North as a guide, we adopt $t = 70$ Myr, Salpeter IMF, $[Z/Z_{\odot}] = -0.7$, and $E(B-V) = 0.15$ as our fiducial parameters.

We then change the age, metallicity, and dust content of this model by various factors and calculate the effect it would have on the UV-continuum slope β predicted for a galaxy, as measured over the baseline 1600–2300 Å. The results are shown in Figure 7. From this figure, it is clear that the largest changes in the UV-continuum slope come from variations in the dust content of galaxies and the other parameters have a smaller effect. For factor of ∼2 changes in the age, metallicity, and dust, we estimate that the UV-continuum slope β change by ∼0.05, ∼0.1, ∼0.35, respectively.

Of course, we also see that age has a modest effect on the observed UV-continuum slope β. This is well documented in the literature (e.g., Bell 2002; Kong et al. 2004; Cortese et al. 2006; Panuzzo et al. 2007). Despite this sensitivity of β to age, no significant change is found in the median ages of star-forming galaxies from $z \sim 6$ to $z \sim 4$ (Stark et al. 2009), and little changes are found in the median ages as a function of luminosity (there is a hint that lower luminosity galaxies may be ∼1.5 times younger). Galaxies are found to have median ages of ∼150 Myr. This suggests that the effect that systematic changes in the age of the stellar populations on the mean β is at most modest ($\lesssim 0.2$). Moreover, even if we ignore these observational results, it seems unlikely that the average ages of star-forming galaxies would increase more rapidly than some multiple of the dynamical time in a galaxy. From theory (e.g., Mo et al. 1998), the dynamical timescale as $\rho^{-1/2} \sim (1+z)^{-3/2}$—which is a factor of ∼3 (0.5 dex) from $z \sim 6$ to $z \sim 2.5$. For such a change in age, the change in β would be $\Delta\beta = 0.2$, which is small compared to the observed differences—where $\Delta\beta$ is 0.5–1.0.

Metallicity has an even smaller effect (by a factor of ∼8) on the observed UV-continuum slopes β than either dust or age do, so we would require very large variations in the metallicity to affect the UV-continuum slope β in any sizeable way. However, since any substantial change in metallicity would almost certainly be accompanied by a similar change in the dust content (given the correlation between these two quantities), we would again be left with a situation where the changes in β resulting from metallicity would be completely overwhelmed by changes in β resulting from dust.

Changing the IMF of galaxies only appears to have a modest effect on the UV-continuum slope β. For example, changing the slope of the IMF by ∼0.5 only changes β by $\lesssim$0.1. Moreover, for a steep enough UV-continuum slope and a top heavy enough IMF, there is very red nebular continuum emission (resulting from the ionizing radiation; Schaerer 2002, 2003; Venkatesan et al. 2003; Zackrisson et al. 2008; Schaerer & de Barros 2009) that more than offsets the very blue spectrum from the stars themselves (Figure 1 from Schaerer & Pelló 2005).

In summary, we expect that the observed variations in the mean UV-continuum slope β to be largely the result of changes in the mean dust extinction.

4.5. Connection to Trends Found in Star-forming Galaxies at $z \sim 0$–3

One of the most salient trends we found in the UV-continuum slopes β derived for $z \sim 2.5$ U-dropout and $z \sim 4$ B-dropout galaxies was the presence of a strong correlation between the UV-continuum slope β and UV luminosity (see also Meurer et al. 1999). As detailed in Section 3.9, the mean UV-continuum slope β for $z \sim 2.5$ and $z \sim 4$ galaxies decreases (becomes bluer) by 0.20 ± 0.04 and 0.15 ± 0.01, respectively, for each magnitude we reach fainter in luminosity.

It seems reasonable to imagine that such trends might also be present in even lower redshift samples or in other colors for $z \sim$ 2–4 samples. In fact, a strong correlation between UV-optical colors and rest-frame optical magnitude has been found for star-forming galaxies in the "blue" cloud (e.g., Papovich et al. 2001, 2004; Baldry et al. 2004; Wyder et al. 2007; Labbé et al. 2007), in the sense that more luminous galaxies are redder. This is very similar to the relationship we find between the UV-continuum slope β and UV luminosity. Looking at the comparison more quantitatively, the slope of the color–magnitude relationship Labbé et al. (2007) measure, for example, is equivalent to $d\beta/dM_{UV}$ of ~ -0.27. This is similar to the -0.20 ± 0.04 slope we estimate at $z \sim 2.5$ for our U-dropout selection (see Section 3.9).

Finally, it is worthwhile to remark on the physical origin of this slope—which could plausibly be explained by changes in either the mean age or the dust content of galaxies as a function of luminosity. In the previous section, we argued that the simplest way of accommodating the sizeable change ($\Delta\beta \sim 0.6$) in the UV-continuum slope β with luminosity was through a change in the dust content of the galaxy population. Explaining the change in β with age would require very large changes (factor of ∼10 changes in the mean galaxy age)—which seem contrary to the modest changes in age noted by Stark et al. (2009) as a function of luminosity.

Labbé et al. (2007) also argue that the slope in the color–magnitude relationship is predominantly the result of a variation in the dust content. Labbé et al. (2007) draw this conclusion based upon an examination of the slope of the color–magnitude relationship versus wavelength and through a detailed examination of the $z \sim 0$ Nearby Galaxy Field Sample (Jansen et al. 2000). This suggests that the color–magnitude relationship we observe for star-forming galaxies may simply be another manifestation of the well-known mass–metallicity relationship observed at $z \sim$0–3 (e.g., Tremonti et al. 2004; Erb et al. 2006a; Maiolino et al. 2008).

5. INFERRED DUST EXTINCTION

In Sections 4.4 and 4.5, we argued that the most likely interpretation of the systematic changes in the mean UV-continuum slope β (as a function of redshift or luminosity) is a change in the dust content of galaxies. Given the sizeable (factor of $\sim$5) dust corrections inferred at $z \sim$2–3 for luminous galaxies (e.g., Reddy et al. 2006; Meurer et al. 1999; Erb et al. 2006b; Reddy & Steidel 2004), any changes in the estimated dust corrections would have a substantial effect on the SFR densities inferred at higher redshifts and hence its evolution across cosmic time.

In this section, we use the measured UV-continuum slope β distribution at $z \sim$ 2–6 to estimate the dust corrections for UV-bright galaxies at $z \sim$ 2–6. We begin by describing the formula we use to estimate dust extinction using the measured UV-continuum slopes (Section 5.1). Then, we discuss the likely significance of the observed trends in UV-continuum slope and dust extinction, versus luminosity (Section 5.2) and redshift (Section 5.3). In Section 5.4, we combine the derived trends in dust extinction with the observed UV LFs to calculate dust corrections, to various limiting luminosities. We then use the typical dust corrections for specific luminosity galaxies to estimate the bolometric luminosities of specific luminosity galaxies in the UV (Section 5.5). Finally, in Section 5.6, we discuss the few well-cited cases of dusty high-redshift galaxies and explain why they do not alter the simple picture we lay out in this section.

5.1. Inferred Dust Extinction

To estimate the effective dust extinction for galaxies in our various samples and as a function of redshift, we rely upon the correlation found between dust extinction and the UV-continuum slope β at $z \sim 0$ (Meurer et al. 1999):

$$A_{1600} = 4.43 + 1.99\beta', \quad (1)$$

where the dust extinction A_{1600} here is specified at rest frame 1600 Å and where β' is the UV-continuum slope measured from 1300 Å to 2600 Å. This relationship has been shown to be a reasonable predictor of the actual dust extinction in galaxies at $z \sim 0$, $z \sim 1$, $z \sim 2$ for all but the youngest (Reddy et al. 2006; Siana et al. 2008, 2009) and most obscured starburst galaxies (e.g., Meurer et al. 1995, 1999; Burgarella et al. 2005; Laird et al. 2005; Reddy et al. 2006), and therefore it is reasonable for us to use this equation to estimate extinction in each of our high-redshift dropout samples. This technique has already been employed in several previous studies estimating the SFR density at $z \sim$ 2–6 (e.g., Adelberger & Steidel 2000; Meurer et al. 1999; Bouwens et al. 2006; Stark et al. 2007).

Of course, there are many reasons for suspecting that Equation (1) may not work very well at early times, both because of the very different ages and metallicities of stellar populations and because the dust itself may have very different characteristics. After all, the standard mechanism for forming dust in the envelopes of asymptotic giant branch (AGB) stars should not work at $z \gtrsim 5$ because the universe is not old enough at these redshifts to have produced AGB stars. Dust in $z \gtrsim 5$ galaxies has therefore been suggested to form by another mechanism, most frequently in supernovae (SNe) ejecta (e.g., Maiolino et al. 2004; Maiolino 2006). Equation (1) is also known to fail at $z \sim 3$ for a few lensed sources (e.g., MS1512-cB58 (Siana et al. 2008) or the Cosmic Eye (Siana et al. 2009)) and for very young (<100 Myr) star-forming galaxies at $z \sim 2$ (Reddy et al. 2006).

To use Equation (1), we need to convert the UV-continuum slopes β we have derived (which have a baseline 1600–2300 Å) to that appropriate for Equation (1) (where β assumes a slightly more extended baseline 1300–2600 Å). We therefore explored the value of the UV-continuum slope over these two different baselines for a wide variety of star formation histories and values of the dust extinction. We found that they are very similar in general, with an absolute difference generally $\Delta\beta < 0.2$. While there is clearly latitude in the precise relationship we use to convert the measured UV-continuum slopes β to this new wavelength, perhaps the least arbitrary set of SEDs to use to perform this conversion is those we use in the Appendix to estimate β from the observed colors. For those SEDs (which assume a $e^{-t/\tau}$ star formation history, $t = 10$ Myr, $\tau = 70$ Myr, $[Z/Z_\odot] = -0.7$, the Calzetti et al. (2000) extinction law, and a Salpeter IMF), we derive the following relationship $\beta' = -2.31 + 1.11(\beta + 2.3)$. While obviously there are some uncertainties in using this conversion, there are at least as many uncertainties in using Equation (1) to estimate the dust obscuration in high-redshift galaxies, and so we will ignore these uncertainties in the subsequent discussion.

5.2. Dependence of Dust Extinction on UV Luminosity

We will first discuss the dependence of the UV-continuum slope and inferred dust extinction on the *UV luminosity*. We find that the UV-continuum slope β shows a strong dependence on the UV luminosity at both $z \sim 2.5$ and $z \sim 4$. This suggests that dust extinction is positively correlated with the observed UV luminosity, in the sense that more luminous galaxies are more dust obscured.

At face value, this trend would appear to be contrary to what Adelberger & Steidel (2000) and Reddy et al. (2008) found in their examination of $z \sim 3$ U-dropouts—where no correlation was found between the UV-continuum slope β and the observed UV luminosity over the range $\mathcal{R} = 22$ ($M_{UV,AB} \sim -23.5$) to $\mathcal{R} = 25.5$ ($M_{UV,AB} \sim -20$). This is a somewhat brighter range than we probe with good statistics, suggesting that dust extinction (and the UV-continuum slope β) may be a weaker function of the observed UV magnitude at $M_{UV,AB} \lesssim -20$ ($\mathcal{R} \lesssim 25.5$) than it is over the whole range probed here. Indeed, using this same magnitude baseline ($V_{606,AB} < 25.5$) and a t test, we only find the correlation between β and UV luminosities to be significant at 75% confidence from our own $z \sim 2.5$ U-dropout sample. Thus, while the correlation would appear to be weaker for the more luminous sources, the existence of a correlation between β and observed UV magnitude over the entire magnitude range probed here is very significant (i.e., $>4\sigma$ result).

In order to understand the differences between our results and those of Adelberger & Steidel (2000), we must appreciate that galaxies exhibit very different behaviors as a function

of UV luminosity, depending upon whether we are dealing with galaxies at higher or lower luminosities. For the lower luminosity regime, a large fraction of the sources should have very low SFRs. Given the well-known correlation between *the SFR* and dust extinction (e.g., Wang & Heckman 1996; Hopkins et al. 2001; Martin et al. 2005; Reddy et al. 2006; Zheng et al. 2007), these galaxies would have low dust extinction (less than $\lesssim 0.2$ mag), and therefore the UV luminosity should be approximately proportional to the SFR. Consequently, we might expect the dust extinction (and UV-continuum slope) to be approximately proportional to UV luminosity at low luminosities. This is what we observe.

In the higher luminosity regime, we might expect the SFR to be much larger in general. We would also expect the dust extinction in these galaxies to be larger, given the correlation of dust extinction with the SFR. As such, any increase in the SFR of a galaxy would be largely offset by a similar increase in the dust extinction—resulting in a very weak correlation between the UV light output from a galaxy and its SFR (or dust extinction). This is exactly what Adelberger & Steidel (2000) and Reddy et al. (2008) found in their sample of luminous ($> 0.3L^*_{z=3}$) $z \sim 3$ U-dropout galaxies. Of course, we would also expect galaxies with very large extinctions to be present in galaxy samples at lower UV luminosities, albeit as a small fraction. We can infer this latter fact from the volume density of such systems: $> 10^{12} L_\odot$ IR ultra-luminous galaxies (e.g., from the $z \sim 2$ IR LF of Caputi et al. 2007) have a much smaller volume density than UV faint sources (by factors of >50; see discussion in Section 8 of Reddy & Steidel 2009). Consequently, we would expect the contribution from such IR ultra-luminous galaxies to the overall SFR density in UV faint samples to be relatively small.

5.3. Dependence of Dust Extinction on Redshift

Very high-redshift ($z \gtrsim 5$) galaxies are also much bluer in general than $z \sim$ 2–4 galaxies of the same luminosity. This suggests that $z \gtrsim 5$ galaxies are less dust obscured as well. This smaller dust obscuration is probably a consequence of an evolution in the relationship between dust extinction and the SFR, such that for a given SFR the observed dust obscuration increases as a function of cosmic time. This would cause higher redshift galaxies of a given UV luminosity to have bluer UV-continuum slopes. Such an evolution in extinction-SFR relationship is observed from $z \sim 2$ to $z \sim 0$ (Reddy et al. 2006; Buat et al. 2007; Burgarella et al. 2007), and it is expected that this relationship continues to evolve from $z \sim 6$. This is presumably a result of the gradual build-up in metals in the universe with cosmic time.

5.4. Average Dust Extinction for LBGs to Specific Luminosity Limits

It is interesting to estimate what the observed distribution of UV-continuum slopes β would imply for the dust extinction, if Equation (1) holds. For this calculation, we assume that we can represent the distribution of UV-continuum slopes β as a simple Gaussian with mean and 1σ scatter as derived earlier in our paper (Table 4; see Section 3.7). We then fold this distribution through Equation (1) to calculate the effective dust extinction integrated down to various limiting luminosities. We adopt the UV LF of Bouwens et al. (2007) at $z \sim 4$, $z \sim 5$, and $z \sim 6$ and that of Reddy & Steidel (2009) at $z \sim 3$ for this calculation.

The effective dust extinction is presented in Table 5 and Figure 8. To a limiting luminosity of 0.3 $L^*_{z=3}$, we infer a dust extinction of 6.0 ± 2.5× (or 1.6 mag) at $z \sim 2.5$, very close to the 5.4 ± 0.9× dust attention Meurer et al. (1999) estimated previously from the UV continuum slopes of HDF-North U-dropouts. It is encouraging that this extinction estimate is very similar to the values estimated at $z \sim 2$ using a wide variety of multiwavelength data and SFR calibrators (e.g., Reddy & Steidel 2004; Reddy et al. 2006; Erb et al. 2006b). However, these extinction estimates are a few times higher than those inferred by Carilli et al. (2008) at $z \sim 3$ by stacking the Very Large Array (VLA) radio observations of $> 0.2L^*_{z=3}U$-dropouts in the COSMOS field (where a factor of 1.8 ± 0.4 extinction was inferred). This may indicate that the Meurer et al. (1999) relationship substantially overestimates the dust extinction at $z > 2$, or it may indicate that the radio luminosity for a given SFR is systematically lower at high redshift (Carilli et al. 2008). At this time, it is not obvious how this issue will be resolved, though it seems clear that dust extinction will be less of a concern as we reach back further in cosmic time (e.g., see Section 6.2).

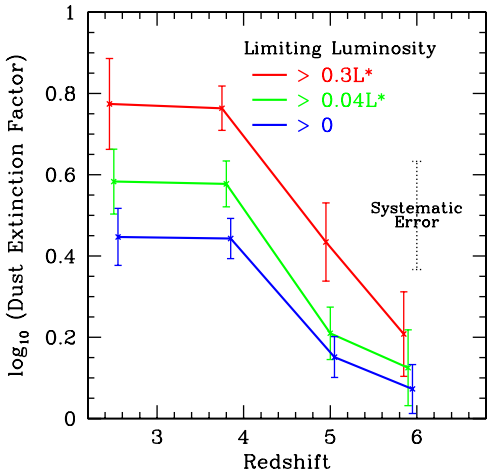

Figure 8. Effective dust extinction (at ∼1600 Å) estimated for LBGs vs. redshift integrated down to a luminosity of $0.3L^*_{z=3}$ (red lines), $0.04L^*_{z=3}$ (green lines), and 0 (blue lines). The precise redshifts at which our dust extinction estimates are presented are shifted slightly to minimize overlap between the different limiting luminosities. The error bars shown here represent the random errors. The dotted error bar included on the right here is the systematic error that likely applies to each dust extinction estimate (based upon our conservative estimate that all β estimates in this paper are uncertain at the $\Delta\beta \sim \pm 0.15$ level). This systematic error is unlikely to have any effect on the trends and differences seen here, but could change the overall scaling. The dust extinctions presented here are also given in Table 5. These extinctions are estimated based upon the distribution of UV-continuum slopes observed (Table 4) and the correlation between UV-continuum slope and dust obscuration observed at $z \sim$0–2 (Equation (1); Meurer et al. 1999). Note that the dust extinctions are much lower when integrated to very low luminosities.

At higher redshifts and integrated down to lower luminosities, the effective dust extinction is much less, i.e., factors of $\lesssim$2–3 ($\lesssim$ 1 mag). Qualitatively, we would expect such a change due to the much bluer UV-continuum slopes β found at these luminosities and redshifts. Nonetheless it is still quite striking how much smaller the estimated dust extinction is when including light from the lowest luminosity galaxies. In detail, this is because lower luminosity galaxies dominate the total luminosity density in the UV continuum (see Figure 9) and the average dust extinction in these lower luminosity galaxies is quite low. Bouwens et al. (2007) estimated that half of the light in the UV-continuum originated in galaxies fainter than 0.06 $L^*_{z=3}$ (~ -18 AB mag; see Figure 9). At ~ -18 AB mag, we find that galaxies have an average UV-continuum slope β of ~ -2 to -2.5.

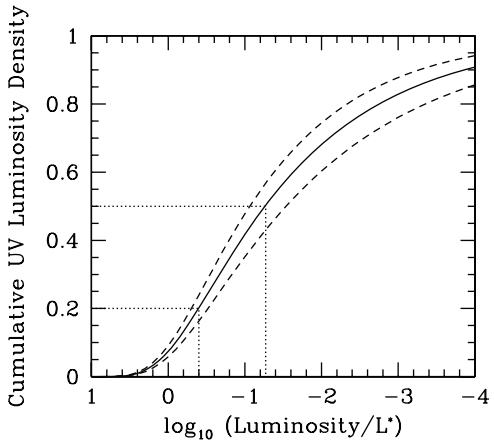

Figure 9. Fraction of the total UV luminosity density that arises from galaxies brighter than a given luminosity (solid line). This calculation assumes the faint-end slope α of -1.73 preferred in recent determinations of the LF at $z \sim 2$–6 (e.g., Yoshida et al. 2006; Bouwens et al. 2007; Oesch et al. 2007; Reddy & Steidel 2009). The dashed lines show the fraction of the luminosity density brighter than specific luminosities for faint-end slopes α of -1.68 and -1.78 (which differ at the 1σ level from the $\alpha = -1.73$ value preferred at $z \sim 4$; Bouwens et al. 2007). Note that $> 50\%$ and $> 80\%$ of the luminosity density occurs in galaxies fainter than $10^{-1.3}L^* \sim 0.05L^*$ and $10^{-0.4}L^* \sim 0.4L^*$, respectively, demonstrating how important it is to understand the dust correction down to very low luminosities.

These dust corrections are much more modest than have occasionally been assumed to calculate the total SFR density at early times, e.g., the factor of ∼8 adopted by Giavalisco et al. (2004b) or the factor of ∼3 adopted by Hopkins (2004) for their common obscuration correction. Previously, Bouwens et al. (2006) and Lehnert & Bremer (2005) have argued that the dust extinction was likely less than a factor of $\lesssim$2 at $z \sim 5$–6 and Reddy & Steidel (2009) argued that when integrated to lower luminosities the dust extinction was less than a factor of ∼1.5–2 at $z \sim 2$–3 (adopting their luminosity_dependent reddening (LDR) model). The Reddy & Steidel (2009) LDR dust extinctions are somewhat lower than what we estimate here, largely because they assume there is little dust extinction for galaxies with luminosities fainter than ~ -18.5 ($0.1\,L^*_{z=3}$). By contrast, the dust extinction we adopt come from the distribution of UV-continuum slopes we find and using Equation (1). While it is unclear which set of dust corrections is most accurate, it seems quite clear that the dust extinction must be very low for galaxies at very low UV luminosities. This follows from two observational findings: (1) the much larger volume density (i.e., $\sim 10^{-2}$ Mpc^{-3}) of galaxies with low UV luminosities than ultra-luminous IR galaxy (ULIRG)-type sources (i.e., where $10^{-3.5}$ Mpc^{-3}) and (2) the correlation between dust extinction and bolometric luminosity (e.g., Wang & Heckman 1996; Hopkins et al. 2001; Martin et al. 2005; Reddy et al. 2006; Buat et al. 2007; Burgarella et al. 2007). As a result of these two findings, we can conclude that essentially all of the galaxies with lower UV luminosities (>99%) do not have very high bolometric luminosities, and therefore do not exhibit large dust extinctions.

5.5. Bolometric Luminosities of Galaxies in Our UV Selections

The viability of the Meurer et al. (1999) IRX-β relationship (Equation (1)) we used to correct the observed UV luminosities for the dust extinction is a strong function of the bolometric luminosity of the sources. For example, Reddy et al. (2006) found that while the Meurer et al. (1999) relationship worked well between $10^{11}L_\odot$ and $10^{12}L_\odot$ at $z \sim 2$, it failed badly for galaxies with luminosities $> 10^{12}L_\odot$ (see also Chapman et al. 2005).

To investigate the validity of the estimates we made in the previous section, it is interesting therefore to estimate the bolometric luminosities for galaxies with specific UV luminosities in our LBG selections. We again take advantage of Equation (1), as well as the relationships between the UV-continuum slope β and UV luminosity (Section 3.9) to make this estimate. This results in the following relationship between the absolute magnitude of a galaxy in the UV and the bolometric luminosity $L_{\rm bol}$ at $z \sim 2.5$:

$$L_{\rm bol} = 10^{11.67-0.58(M_{UV,AB}+21)}L_\odot. \quad (2)$$

The relationship at $z \sim 4$ is similar. We emphasize that this relationship does not generally hold for galaxies where $L_{\rm bol} > 10^{12}L_\odot$ (e.g., Reddy et al. 2006; Chapman et al. 2005) or for galaxies which are particularly young (Reddy et al. 2006), because of difficulties in using the UV-continuum slope β to correct for dust extinction in these cases.

The above result is shown in Figure 10 with the red lines for the $z \sim 2.5$ and $z \sim 4$ samples. The hatched region shows the approximate scatter expected in the bolometric luminosity for a given UV luminosity as a result of scatter in the UV-continuum slope β. Also shown are the bolometric luminosities for individual dropout galaxies in the two samples, after correcting their UV luminosities for dust extinction using their measured β's and Equation (1).

From Figure 10 and Equation (2), it seems clear that we would expect a substantial fraction of our dropout sample to have bolometric luminosities less than $10^{12}L_\odot$. As such, we can plausibly make use of the IRX-β relationship to predict the mean dust extinction in galaxies—as we have done in the previous section. Of course, we might expect a few $> 10^{12}L_\odot$ dust-obscured galaxies to be present in the normal dropout samples, with typical UV luminosities and UV-continuum slopes β where Equation (2) may not apply (e.g., Chapman et al. 2005). However, given that the volume density of such galaxies is observed to be much lower ($>$ 10–100×) than that of typical dropout galaxies, we would expect Equation (2) to be reasonably accurate in most cases.

Examining Figure 10, it is certainly quite striking that $z \sim 2$–4 LBGs start becoming extraordinarily rare brightward of ~ -21 or -22, at precisely the same luminosities (i.e., $> 10^{12}L_\odot$) as we expect dust extinction to become increasingly important in galaxies. This suggests the abrupt cut-off in the UV LF at $z \sim 2$–4, i.e., L^*_{UV}, is set by dust extinction—or more precisely the luminosity at which dust obscuration becomes so significant as to offset the increase in energy output from stars. We can examine this by using the observed correlation between dust extinction and bolometric luminosity in the blue star-forming population at $z \sim 2$ (Reddy et al. 2006) $\log L_{\rm bol} = (0.62\pm0.06)\log\frac{L_{\rm IR}}{L_{1600}} + (10.95\pm0.07)$ and applying it in Figure 10. Adopting the observed scatter of $\Delta\log\frac{F_{\rm IR}}{F_{UV}} \sim 0.4$, we show the envelope of M_{UV} and $L_{\rm bol}$ values expected for a wide range in $L_{\rm bol}$. It seems clear from this exercise that we would not expect galaxies to have UV luminosities much brighter than -22 AB mag ($\sim 2\,L^*_{UV}$) and that dust effectively sets the cut-off in the UV LF. This may explain why the value of L^*_{UV} (e.g., Steidel et al. 1999; Reddy et al. 2008) does not evolve much from $z \sim 4$ to $z \sim 2$.

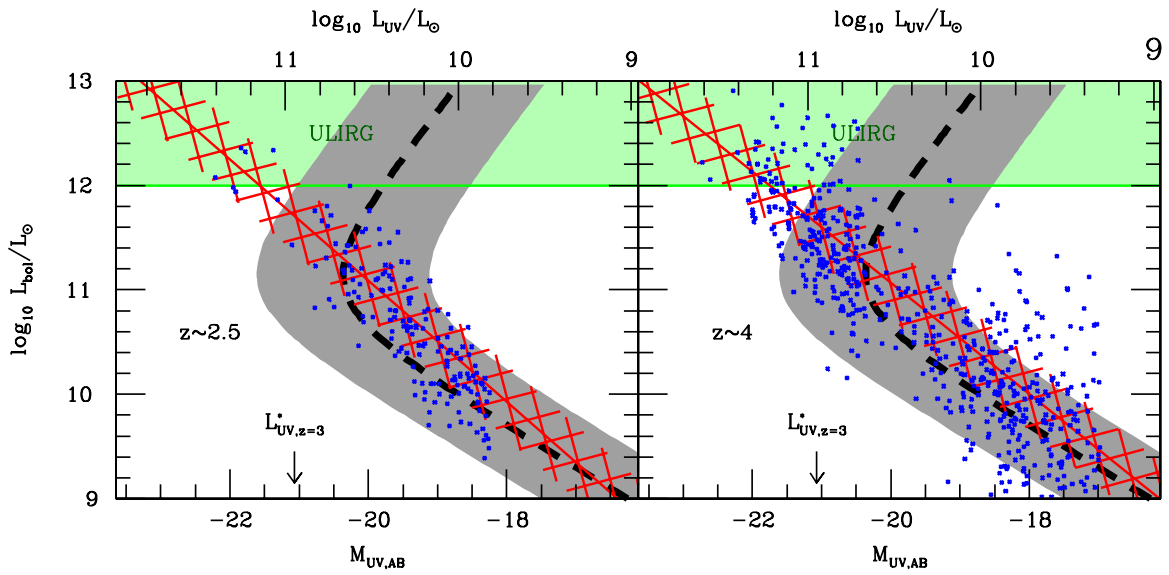

Figure 10. Bolometric luminosity vs. observed UV luminosity $M_{UV,AB}$. The top axis gives this UV luminosity in units of $L_\odot$. The blue points give the UV luminosities and equivalent bolometric luminosities (after dust correction) for individual sources in our $z \sim 2.5$ U-dropout and $z \sim 4$ B-dropout samples (see Figure 3). The dust correction utilizes the observed UV-continuum slopes β and the Meurer et al. (1999) IRX-β relationship. Note that the red line is not a direct fit to the blue points (see Section 3.7 and Figure 3). The red line shows the expected relation between bolometric luminosity and UV luminosity using the luminosity-dependent dust correction derived in Section 5.5 (see Equation (2)). These luminosity-dependent dust corrections are derived utilizing the correlation between UV-continuum slope β and $M_{UV,AB}$ we found for $z \sim 2.5$ U-dropouts and $z \sim 4$ B-dropouts (see Section 3.9) and the Meurer et al. (1999) relationship. The hatched red region indicates the expected 1σ scatter in the bolometric luminosities for a given UV luminosity (based upon the observed scatter of ~0.4 in the UV-continuum slope at a fixed UV luminosity). Since it is unclear whether the Meurer et al. (1999) IRX-β relationship can be accurately used to estimate extinctions for galaxies with $> 10^{12} L_\odot$ luminosities (e.g., Chapman et al. 2005; Reddy et al. 2006), caution should be used in interpreting the blue points or red lines which extend beyond $10^{12} L_\odot$ (green shaded region). The black dashed line shows the relationship between UV luminosity and β that one would derive utilizing the correlation Reddy et al. (2006) found between bolometric luminosity and dust obscuration (see Section 5.5). The shaded gray region corresponds to a ~0.4 dex scatter in the dust obscuration. Notice how the population of bluer, more dust-free dropout galaxies in our selections span a wide range in bolometric luminosity, extending all the way from $10^9 L_\odot$ to $10^{12} L_\odot$ where the LBG population transitions to a more dust-obscured ULIRG-like population. It is quite interesting that the UV luminosity where galaxies begin reaching bolometric luminosities of $\sim 10^{12} L_\odot$—where dust obscuration becomes very important—is very close to $L^*_{z=3}$ (Steidel et al. 1999; shown in the figure). The UV LF therefore begins to cut off at precisely the same luminosities as dust obscuration is becoming increasingly important in attenuating the light. This suggests that the value of L^* at $z \sim 2$–4 may be set (in part) by the luminosities at which dust obscuration becomes dominant. It may also help to explain the mild evolution in the UV LF from $z \sim 4$ to $z \sim 2$ (see Section 5.5).

5.6. High-redshift Galaxies from the Literature that Would Seem to Show Substantial Dust Extinction

The dust extinctions we infer are substantially less than have been inferred in some studies of specific high-redshift galaxies. One such example is the $z = 6.56$ galaxy behind Abell 370 (HCM6A; Hu et al. 2002). This source was found to have a significantly larger flux in the 4.5 μm band than in the 3.6 μm band—which may be due to substantial $H\alpha$ emission falling within the 4.5 μm band (Chary et al. 2005). If $H\alpha$ is in fact the explanation, the inferred SFR for this source from this $H\alpha$ emission is ~10 times higher than would be inferred from the UV or Lyα emission alone. Detailed stellar population modeling on the optical, near-IR, and Infrared Array Camera (IRAC) imaging data of HCM6A suggest an extinction factor of ~11× ($A_{UV} = 2.6$ mag) which is much larger than what we infer on average for $z \sim 6$ i-dropouts (Chary et al. 2005; Schaerer & Pelló 2005; see Table 5). However, in subsequent and much deeper IRAC observations of HCM6A (K. Lai et al. 2009, in preparation), no significant difference between the fluxes of HCM6A in the 3.6 μm and 4.5 μm bands is found, leaving us with no reason to believe this source shows significant Hα emission and hence no reason to suspect that its UV light is significantly obscured. Direct observations of this source with the MAMBO-2 bolometric array at 1.2 mm also set useful upper limits on its dust obscuration (Boone et al. 2007).

Other examples might include the many high-redshift QSOs discovered by the Sloan Digital Sky Survey (SDSS; Fan et al. 2006). The inferred dust masses of SDSS QSOs can be quite substantial (e.g., J1148+5251; Bertoldi et al. 2003), providing clear evidence that specific high-redshift sources *can* show modest to sizeable dust extinction. Nonetheless, we would not expect QSOs like J1148+5251 to be representative of $z \sim 6$ galaxies, associated as they are with very massive halos and thus in very rich environments. Galaxies in such environments are known to show much greater evolution than galaxies in more typical environments (e.g., Tanaka et al. 2005) and hence much greater metal enrichment.

6. POSSIBLE IMPLICATIONS FOR THE STAR FORMATION HISTORY

In Section 5, we used the observed distribution of UV-continuum slopes β to estimate the dust extinction in star-forming galaxies at $z \sim 2$–6. In the current section, we apply these dust extinctions to UV LFs derived at $z \sim 2$–6 to estimate the SFR density from typical star-forming galaxies (Section 6.1). In Section 6.2, we use recent search results for ULIRGs to estimate their likely contribution to SFR density (since they will not be accurately accounted for by the dust-corrected LBG results). In Section 6.3, we use these two results to estimate the bolometric flux from SFR to be output in the UV and IR. Finally, in Section 6.4, we put together these results to estimate the SFR density from all star-forming galaxies at $z \sim 2$–6.

6.1. The Inferred Star Formation Rate Density at $z \sim 2$–6

It makes sense for us to use the effective dust extinction inferred in the previous section (Table 5) to revise our estimates the SFR density at $z \sim 2$–6. As per our calculation above, we adopt the UV LFs derived by Reddy & Steidel (2009) at $z \sim 3$ and Bouwens et al. (2007) in calculating the SFR densities. In order to convert luminosities in the UV into estimates of the SFR we use the transformation presented by Madau et al. (1998; see also Kennicutt 1998):

$$L_{UV} = \left(\frac{\mathrm{SFR}}{M_{\odot}\mathrm{yr}^{-1}}\right) 8.0 \times 10^{27} \mathrm{erg\,s^{-1}\,Hz^{-1}}, \quad (3)$$

where a 0.1–125 $M_{\odot}$ Salpeter IMF and a constant SFR of $\gtrsim$ 100 Myr are assumed. Conversion to a Kroupa (2001) IMF would result in factor of ∼1.7 smaller SFR estimates.

In view of the young ages (∼ 10–50 Myr) inferred for many star-forming galaxies at $z \sim 5$–6 (e.g., Yan et al. 2006; Eyles et al. 2007; Verma et al. 2007), it is clear that adopting a simple formula like Equation (3) (which requires the assumption of $\gtrsim$ 100 Myr ages) would result in a systematic underestimate of the SFR density of the universe at very early times (e.g., Verma et al. 2007; Reddy & Steidel 2009; Stanway et al. 2005). In any case, given our uncertain knowledge of how the age distribution of star-forming galaxies varies as a function of redshift and luminosity, it is difficult to know precisely how much we must revise our estimates upward. Working with a sample of bright $z \sim 5$ galaxies, Verma et al. (2007) estimate that the actual SFRs may be twice as large as what Equation (3) would suggest. Of course, this effect may be partially offset by the fact that for these same young star-forming systems that standard dust corrections (e.g., following Meurer et al. 1999) seem to overpredict the SFRs by factors of $\gtrsim$2 (Reddy et al. 2006; Siana et al. 2008). In any case, going forward, we will need to obtain tighter constraints on the age distribution of galaxies as a function of redshift and especially to very low luminosities (since faint galaxies provide the dominant contribution to the SFR density).

Our results are presented in Figure 11 and Table 6. These dust-corrected SFR densities are somewhat lower than presented by Bouwens et al. (2008). This is because the average dust extinction including the lowest luminosity galaxies is less than when only considering L^* galaxies. We will discuss these results in more depth in Section 6.4 after including the contribution from ULIRGs.

6.2. Contribution of ULIRGs to the Star Formation Rate Density at $z \sim 2$–6

Of course, we would expect the extinction estimates above to underestimate the effective extinction, given that Equation (1) does not accurately describe galaxies with very high SFRs, dust extinctions, and bolometric luminosities (e.g., Elbaz et al. 2007), particularly those systems where $L_{\mathrm{bol}} > 10^{12} L_{\odot}$. The SFR from such galaxies can be better accounted for by a direct consideration of IR LFs (e.g., Caputi et al. 2007).[11] Reddy & Steidel (2009) have already performed such a calculation at $z \sim 2$, integrating the $z \sim 2$ IR LF of Caputi et al. (2007) down to bolometric luminosities of $10^{12} L_{\odot}$.[12] Reddy & Steidel (2009) infer an SFR density of 0.03 $M_{\odot}$ yr^{-1}Mpc^{-3} (Kroupa IMF) at $z \sim 2$ from this population. Obviously, there are some modest uncertainties as to the exact bolometric luminosity down to which one should integrate the Caputi et al. (2007) LF (to correct for the ULIRG population not reasonably accounted for by the Meurer et al. 1999 relation), and so this SFR density could be larger. For example, assuming we integrated the Caputi et al. 2007 LF down to $10^{11.8} L_{\mathrm{bol}}$ instead, the ULIRG contribution could increase by ∼50%.

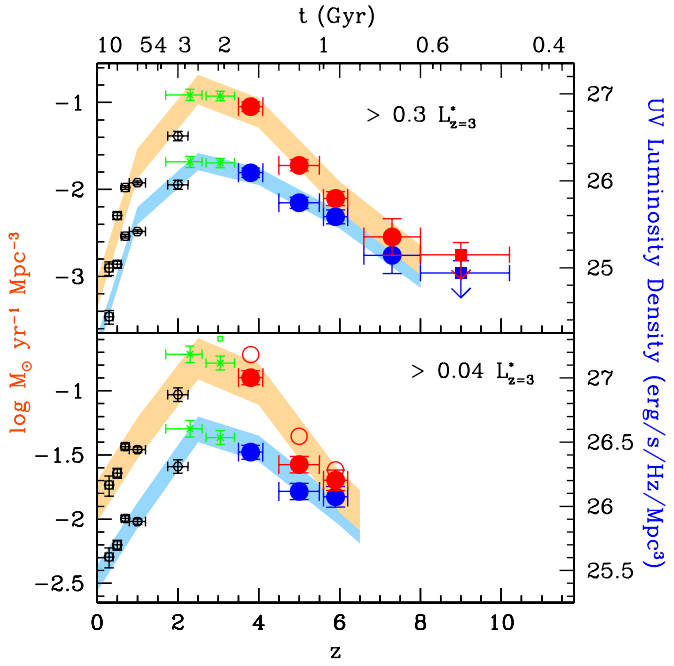

Figure 11. Star formation history inferred using the dust corrections determined here (upper set of points; orange shaded region) and without those dust corrections (lower set of points; blue shaded region). These dust corrections (Table 5) are applied to the luminosity density determinations at $z > 2$ by Reddy & Steidel (2009), Bouwens et al. (2007, 2008). Otherwise, the dust corrections of Schiminovich et al. (2005) are assumed. The top panel is based upon the total UV luminosity density integrated to 0.3 $L^*_{z=3}$ and the bottom panel is based upon the total UV luminosity density integrated to 0.04$L^*_{z=3}$. The rest-frame UV continuum luminosity density is converted to a SFR density assuming a constant $> 10^8$ yr star formation model and a Salpeter (1955) IMF (Madau et al. 1998). Conversion to a Kroupa (2001) IMF would result in a factor of ∼1.7 (0.23 dex) decrease in the SFR density estimates given here. Assuming younger ages for star-forming galaxies in high-redshift samples would increase the SFR density estimates by a similar factor (Verma et al. 2007). Shown are the luminosity density determinations by Schiminovich et al. (2005; black hexagons), Reddy & Steidel (2009; green crosses), Bouwens et al. (2007; blue/red circles), and Bouwens et al. (2008; blue/red circles and 1σ upper limit). The open symbols show the SFR densities that would be inferred if we applied the same dust correction to $> 0.04L^*_{z=3}$ as we apply to $> 0.3L^*_{z=3}$. It is clear then that ignoring the fact that lower luminosity galaxies have much lower values for the dust extinction will result in an overestimate of the SFR density. See also Table 5. Table 5 and Figure 10 from Reddy & Steidel (2009) make a similar point. The equivalent SFR density (UV luminosity density) is also shown assuming no extinction correction (lower set of points).

[11] While there has been some suggestion that galaxies whose IR luminosities exceed that predicted by the IRX-β relationship fail due to a contribution from an obscured AGN (e.g., Daddi et al. 2007) and therefore the SFR derived from the IRX-β is correct after all, it has been found (e.g., Murphy et al. 2009) that this is only partially the explanation, and that part of the IR excess would appear to be due to star formation. We therefore consider it safer to include the contribution from $> 10^{12} L_{\odot}$ IR-luminous galaxies explicitly through the use of IR surveys.

[12] There has been sizeable variation in the literature in the relationships used to convert from 24 μm fluxes to the bolometric flux in the IR (e.g., Bavouzet et al. 2008 versus that implied by the Chary & Elbaz 2001 templates found to work in the local universe), and therefore large differences in the reported LFs in the IR (e.g., Pérez-González et al. 2005 versus Caputi et al. 2007). Fortunately, the situation seems to have become more clear from the observations, and Caputi et al. (2007) adopt an apparently more justified linear relationship (Bavouzet et al. 2008) to convert between the 24 μm flux and the bolometric IR flux.

Despite the existence of these possible uncertainties, we adopt as our baseline values at $z \sim 2.5$ the contribution Reddy & Steidel (2009) derived from the $z \sim 2$ Caputi et a. (2007) IR LF. We therefore correct our SFR density estimates at $z \sim 2.5$ in Table 6 for this population. The results are given in the lower section of Table 7. The obscured population only has a modest effect on the dust extinction (and SFR density), increasing it by ∼20% (see also discussion in Reddy & Steidel 2009).

Accounting for the effect of such ULIRGs on the SFR density (and extinction estimates) at $z \gtrsim 4$ is a much less certain enterprise. Not only is it difficult to probe to moderate luminosities with current instrumentation, but conducting follow-up observations on specific $z \gtrsim 4$ sources (e.g., to determine redshifts) is also quite challenging at present. As a result, only a handful of high quality $z \gtrsim 4$ ULIRG candidates (e.g., Capak et al. 2008; Daddi et al. 2009; Wang et al. 2009; Schinnerer et al. 2008; Dunlop et al. 2004) currently exist, and essentially all of them are at $z \sim 4$. Perhaps the deepest, most well-defined selection of such sources is found in the deep ∼50–100 arcmin^2 submillimeter SCUBA field lying within the HDF-North GOODS area (Pope et al. 2006). We will use those $z \sim 4$ sources to set a lower limit on the contribution of highly obscured galaxies to the SFR density at $z \sim 4$. Starting with the ∼5–8 ULIRGs within this field that are plausibly at $z \sim 4$ (e.g., Daddi et al. 2009; Mancini et al. 2009) and then dividing by the comoving volume at $z \sim 4$, one derives an SFR density of ∼0.01–0.02 $M_\odot \mathrm{yr}^{-1}\mathrm{Mp}^{-3}$ (depending upon what fraction of the candidates are actually at $z \sim 4$). Again, we can correct our $z \sim 4$ SFR density estimates for this population. Not surprisingly, this population only contributes ∼10% to the SFR density (see Figure 14).

Of course, we might expect there to be highly obscured galaxies below the $10^{12}\ L_\odot$ luminosity limits that also contribute substantially to the SFR density relevant to these probes, so one might argue that 10% is just a lower limit. However, as we have already argued, we should be able to account for the star formation of these lower luminosity systems from LBG selections. The results of Reddy et al. (2006) suggest that the UV-corrected SFRs of galaxies can be accurately estimated at $z \sim 2$ to $10^{12} L_\odot$, and we would expect these corrections to be even easier to perform at $z \sim 4$ than at $z \sim 2$—given the trend of high-redshift galaxies to show less and less dust extinction at a fixed SFR at increasingly high redshifts (e.g., Reddy et al. 2006; Buat et al. 2007; Burgarella et al. 2007).

Given that $> 10^{12} L_\odot$ ULIRGs only contribute ∼20% of the SFR density at $z \sim 2$–3 and perhaps ∼10% at $z \sim 4$, one might expect the contribution of such a population at $z \sim 5$–6 also to be quite small. We can obtain a crude estimate of this fraction, if we assume that IR luminous galaxies have a bolometric LF similar to that derived by Caputi et al. (2007) at $z \sim 2$ (i.e., where $L^*_{\mathrm{bol}} = 10^{11.8\pm0.1}$) and then evolve in a very similar way to the UV LF at $z \geqslant 3$. We therefore assume that L^*_{bol} scales with redshift as $10^{-0.4(0.35(z-3))} \sim (1/1.38)^{z-3}$ to match the observed $M^*_{UV}(z) = M^*_{UV}(z = 4) + 0.35(z - 4)$ evolution in the UV LF from $z \sim 4$ to $z \sim 7$ (e.g., Bouwens et al. 2007, 2008).[13] We then compare the fractional SFR density in $L_{\mathrm{bol}} > 10^{12} L_\odot$ galaxies with that from the star-forming population as a whole. We find that the fractional SFR density in ULIRGs is 6% at $z \sim 5$ and 2% at $z \sim 6$. For these assumptions, the fractional SFR density in $L_{\mathrm{bol}} > 10^{12} L_\odot$ galaxies is 23% and 10% at $z \sim 3$ and $z \sim 4$, respectively, which would seem to be a good match to the observations. We emphasize that this very low ULIRG estimate at $z \gtrsim 5$ is consistent with the lack of very red UV-continuum slopes β at $z \sim 5$–6 (Figure 6; which is in contrast to the tail toward redder (i.e., ~ -1 to 0) β's at $z \sim 4$).

Recent work on GRBs provide strong support for the general conclusion that highly obscured ULIRGs contribute at most a small fraction of the SFR density at $z \gtrsim 4$. Since GRBs are perhaps a good tracer of massive star formation in the high-redshift universe (e.g., Yüksel et al. 2008; Li 2008; Kistler et al. 2009) and may not be biased to lower metallicity environments (Prochaska et al. 2007), we would expect GRBs to occur in galaxies roughly in proportion to their share of the star formation activity in the high-redshift universe. Follow-up work done on GRB host galaxies show that these systems are quite faint at both rest-frame UV (Chen et al. 2009) and optical wavelengths (Chary et al. 2007a). We can therefore conclude that most of the star formation at high redshift occurs in galaxies that are similarly faint.

6.3. Fractional Light Output in the UV and Mid-IR/Far-IR

Before using the extinction estimates for LBG samples (Table 5; Section 5.4) and the aforementioned estimates of the ULIRG contribution (Section 6.2) to estimate the SFR density, we first use them to assess the relative flux output from galaxies in the UV and that output in the mid-IR/far-IR, after dust reprocessing. This entire topic is important in thinking about how best to nail down the SFR density and energy output in the high-redshift universe and for our thinking about the contribution of the high-redshift universe to the extragalactic background light.

In calculating the relative flux output in the UV and mid-IR/far-IR, we assume that essentially all the light from the ULIRG population is emitted in the mid-IR/far-IR and adopting the extinction estimates from Table 5 for the LBG population. We include a plot of this fraction versus redshift in Figure 12. Not surprisingly the majority of the light output from star-forming galaxies at $z \sim 2.5$–4 occurs in the mid-IR/far-IR (after dust reprocessing) as has been emphasized repeatedly (e.g., Hughes et al. 1998; Pérez-González et al. 2005). However, as we will note in Section 6.4, it appears that we can account for most of this energy output using the LBG population. Again, the situation appears to be quite different at $z \gtrsim 5$, with most of the light output occurring in the UV.

6.4. The Star Formation Rate Density at $z \sim 2$–6 Including ULIRGs

Including the contribution from highly obscured ULIRGs (Section 6.2) in with that derived from the UV LFs (Table 6 and Figure 11), our best estimates for the SFR densities are given in Table 7 and Figure 13. The ULIRG population increases the SFR density estimated at $z \sim 2.5$ and $z \sim 4$ (to faint limits) by ∼20% and 10%, respectively. We show the fractional contribution of ULIRGs to the SFR density at $z \sim 2$–6 in Figure 14.

The present dust-corrected SFR densities are less than has been considered in many previous studies. This is largely because many previous studies corrected the SFR density by factors of ∼5–8 times (e.g., Giavalisco et al. 2004b)—which is the dust correction relevant for L^* galaxies. This has

[13] Note that here we are implicitly assuming that L^*_{bol} evolves from $z \sim 4$ to $z \sim 3$ despite the lack of evolution in L^*_{UV} over this redshift range (e.g., Reddy et al. 2008). Such a brightening in L^* would be a natural continuation of the evolution in the UV LF from $z \sim 7$ to $z \sim 4$ (e.g., Bouwens et al. 2008). The reason we may not observe this brightening in L^*_{UV} (i.e., the UV LF) beyond $z \sim 4$ is because of the increasing importance of dust extinction in the most bolometrically luminous galaxies (e.g., see Section 5.5).

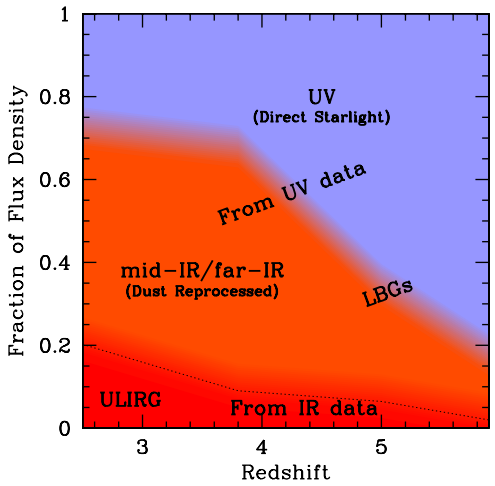

Figure 12. Fraction of the total luminosity density from stars at $z \sim 2$–6 emitted by galaxies in the rest-frame UV and in the mid-IR/far-IR (after dust reprocessing). In calculating the energy output in the UV vs. IR, we adopt the extinction estimates in Table 5 and assume that the total energy output from ULIRGs occurs in the infrared (see Section 6.3). A dotted line is included to show the relative contribution of LBGs and ULIRGs to the mid-IR/far-IR energy output. The contribution of star-forming galaxies is included all the way down to zero luminosity. Most of the energy output at $z \sim 2$–4 would appear to occur in the IR, while at $z \gtrsim 5$ the energy output occurs mostly in the UV. Note that despite most of the energy output at $z \sim 2.5$–4 occurring at IR wavelengths, the SFR densities we derive from LBG surveys (after dust corrections) should account for $\gtrsim 80\%$ of the SFR density at $z \gtrsim 3$ (see Figure 14).

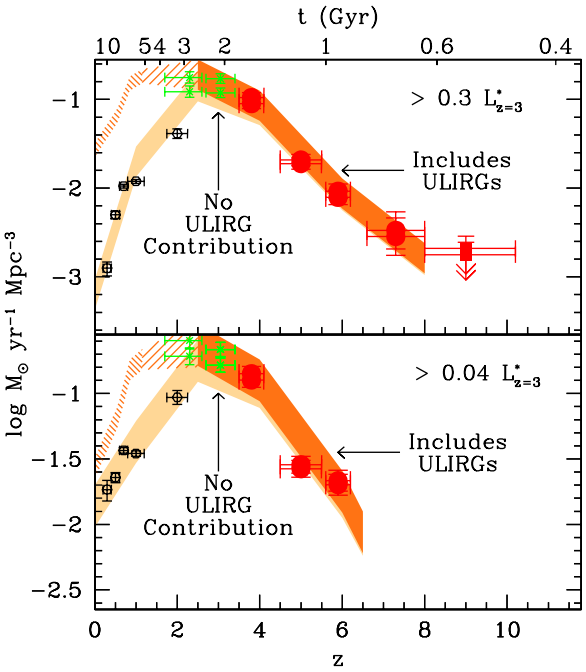

Figure 13. Star formation history inferred with (upper set of points, darker orange contours) and without (lower set of points, lighter orange contours) a contribution from highly obscured ultra-luminous infrared bright ($> 10^{12} L_{\odot}$) galaxies. Otherwise similar to Figure 11. The top panel is based upon the total UV luminosity density integrated to 0.3 $L^*_{z=3}$ and the bottom panel is based upon the total UV luminosity density integrated to $0.04 L^*_{z=3}$. At $z \sim 2.5$, we follow Reddy & Steidel (2009) in using the $z \sim 2$ IR LF of Caputi et al. (2007) to include the contribution from these ULIRGs, while at $z \sim 4$, we estimate their contribution based upon ~5–8 good $z \sim 4$ ULIRG candidates (see Daddi et al. 2009) within the HDF-North GOODS SCUBA supermap (Pope et al. 2006). See also Table 7 and Section 6.2. The darker orange contours at z ~0–1.2 show the SFR density derived using the deepest mid-IR/far-IR observations over the GOODS and Far Infrared Extragalactic Legacy (FIDEL) fields (Magnelli et al. 2009). While IR bright galaxies appear to add significantly to the SFR density at low redshift in the upper panel, this is because the lower set of points/orange contours only include galaxies at the bright end of the UV LF (corresponding to the $0.3 L^*_{z=3}$ limit) and the UV LF there cuts off at much fainter magnitudes than at higher redshifts (compare this situation to the lower panel where the contribution of the mid-IR/far-IR galaxies is much less on a percentage basis). From this figure, it is clear that the contribution of the luminous IR sources to the total SFR density at $z > 2$ is only modest (see also Figure 14).

important implications for studies (e.g., Hopkins & Beacom 2006) featuring comparisons of the stellar mass density with the SFR density.

The claim has been that the SFR density—after integration—exceeds the stellar mass density by factors of ~3–4 (e.g., by Hopkins & Beacom 2006; Wilkins et al. 2008). Adopting a small dust correction (as is appropriate including the effect of the lower luminosity galaxies) substantially reduces the inferred SFR density at high redshift (by factors of ~1.1, ~1.1, ~2.1, and ~2.5 at $z \sim 2.5$, $z \sim 4$, $z \sim 5$, and $z \sim 6$, respectively relative to that used by Wilkins et al. 2008). This should help somewhat to resolve the apparent discrepancy in comparisons with the stellar mass density inferred at high redshift (see also discussion in Reddy & Steidel 2009). Another consideration that may help in this regard is the stellar mass in lower luminosity galaxies. Reddy & Steidel (2009) argue that a consideration of the SFR density and stellar mass densities to the same limiting luminosities largely resolves the apparent discrepancy between the inferred stellar mass density and that obtained by integrating SFR history (approximately doubling the inferred stellar mass densities at $z \sim 2$–3).

What stands out in the above discussion is the role of lower luminosity galaxies and their apparently sizeable contribution to various volume-averaged quantities such as the SFR density and stellar mass density. Clearly, any reasonable examination of these quantities (or comparisons between the stellar mass density and the integral of the SFR density) must accurately account for this population or risk ignoring those galaxies that are most central to making sense of the cosmic evolution.

7. SUMMARY

We use the deep optical and near-IR imaging data over the HUDF and other deep, wide-area fields to quantify the distribution of UV-continuum slopes β (i.e., $f_\lambda \propto \lambda^\beta$) for star-forming galaxies over a wide range in redshift ($z \sim 2$–6) and luminosity ($0.1\, L^*_{z=3}$ to $2\, L^*_{z=3}$). $z \sim 2$–6 galaxies are selected through a U-, B-, V-, and i-dropout technique while UV-continuum slopes (1600–2300 Å rest frame) are derived from the optical and near-IR broadband colors. We then corrected the distribution of UV-continuum slopes for observational selection and photometric errors and tabulate these slopes as a function of both redshift and luminosity (Table 4 and Figure 3). We then discuss possible interpretations of the trends we find (Section 4).

Our conclusions are as follows:

1. The UV-continuum slope distribution of UV bright $L^*_{z=3}$ galaxies over the range $z \sim 2$–6 has a mean β ranging from -1.2 to -2.4, with a dispersion of ~0.4 (Table 4 and Figure 3). As found in previous studies, we find that the mean UV-continuum slope β is bluer (by ~0.5) at $z \sim 6$ than it is at z ~3–4. We also find that the mean UV-continuum slope β is bluer (by ~0.5) at lower luminosities than it is at higher luminosities (see also Meurer et al. 1999). In doing so, we establish the following correlation between β and $M_{UV,AB}$ (Section 3.9); $\beta = (-0.20 \pm 0.04)(M_{UV,AB} + 21) - (1.40 \pm 0.07 \pm 0.15)$ at $z \sim 2.5$ and $\beta = (-0.15 \pm 0.01)(M_{UV,AB} + 21) - (1.48 \pm 0.02 \pm 0.15)$

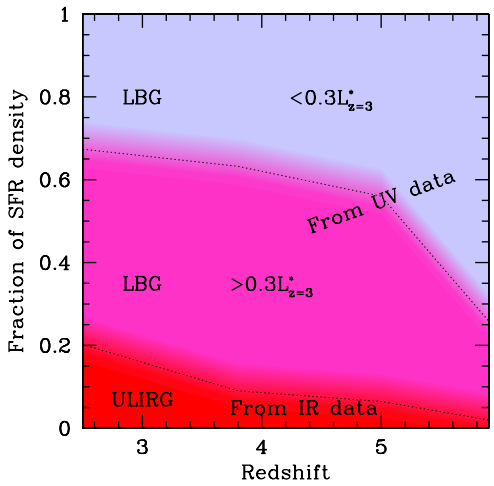

Figure 14. Fraction of the total SFR density at high redshift in lower luminosity LBGs ($< 0.3L^*_{z=3}$), higher luminosity LBGs ($> 0.3L^*_{z=3}$), and ULIRGs ($> 10^{12} L_\odot$). While there will obviously be some overlap between LBG and ULIRG selections, we consider the ULIRG population here separately since mid-IR/far-IR data are required to fully account for the SFR in these galaxies. The contribution of star-forming LBGs is included all the way down to zero luminosity. These fractions are derived based upon the discussion in Sections 5.4, 6.1, and 6.2, and estimates in Tables 6 and 7 and Figures 11 and 13. It is clear that virtually all the SFR densities at $z \gtrsim$3-4 can be accounted for from LBG selections.

at $z \sim 4$. The present quantification of these distributions is essential for accurate LF determinations at high redshift (see Section 4.3).

2. The dropout color selections identify star-forming galaxies at $z \sim$ 2–6 with UV-continuum slopes β as red as $\beta \sim 0.5$ (see Figures 2 and 4). By contrast, the distribution of UV-continuum slopes β that we observe has a mean value of ~ -1.2 to -2.4 with a 1σ dispersion of 0.4—bluer than the color selection limit (i.e., $\beta \sim$0.0–0.5) by $\Delta\beta \gtrsim 1.5$. If the distribution of UV-continuum slopes has a simple form (i.e., has only a single mode), this suggests that our high-redshift dropout selections are largely complete (see also Section 4.1 in Bouwens et al. 2007), and there is not a large population of dust-reddened galaxies at $z \gtrsim 4$. This deficit of red galaxies is particularly prominent relative to the selection function at $z \gtrsim 5$ (see Figure 6, Section 4.2). Independent evidence for this come from Balmer break selections at $z \sim$3–4.5 (which are biased towards older and more massive galaxies) where the distribution of UV-continuum slopes β is also found to be quite blue (Brammer & van Dokkum 2007; see Section 4.2).
3. Stellar population models were used to investigate the effects that changes in dust, age, metallicity, and IMF would have on the UV-continuum slope β. We found that a factor of $\sim$2 (0.3 dex) decreases in the dust, age, and metallicity would make the UV-continuum slope β bluer by $\sim$0.35, $\sim$0.1, and $\sim$0.05, respectively. Changing the slope of the IMF of galaxies by $\sim$0.5 from Salpeter has a minimal effect, changing β by $\lesssim$0.1. The UV-continuum slope β appears to be most sensitive to changes in the dust extinction. Dust is likely to be the most significant cause for changes in β as a function of redshift and luminosity (Section 4.4).
4. Assuming that the observed correlation between dust extinction and UV-continuum slope β at $z \sim$0–2 (e.g., Meurer et al. 1995, 1999; Burgarella et al. 2005; Laird et al. 2005; Reddy et al. 2006; Dale et al. 2007) holds out to $z \sim 6$, we estimate the probable dust extinction in $z \sim$ 2–6 LBG selections (see Table 5). For $> 0.3L^*_{z=3}$ galaxies at $z \sim 2.5$, our estimate is 6.0 ± 2.5—very similar to the values derived by Reddy et al. (2006) and Erb et al. (2006b) using a variety of different multiwavelength data and SFR calibrators, but $\sim$3 times higher than Carilli et al. (2008) estimated for $>0.2L^*_{z=3} z \sim 3$ U-dropouts by stacking radio observations over the COSMOS field. At $z \sim$ 5–6 and to much lower luminosities ($> 0.04L^*_{z=3}$), the inferred dust extinction is much less, i.e., $\lesssim$2–3 times.
5. Since lower luminosity galaxies dominate the luminosity density in the UV at $z \gtrsim 2$ (Bouwens et al. 2006, 2007; Yan & Windhorst 2004; Beckwith et al. 2006; Reddy & Steidel 2009; see Figure 9), establishing the dust extinction of lower luminosity galaxies is crucial for estimates of the total SFR density. As a result of the very low dust extinctions inferred for lower luminosity galaxies, we expect the average dust extinction for the star-forming population at $z \sim$ 2–6 integrated to very low luminosities to be quite small ($\lesssim$2 times; see Table 5). This is similar to what Reddy & Steidel (2009) concluded from the observations and various physical arguments (see Table 5 and Figure 10 from that work).
6. We establish a conversion between UV luminosities and bolometric luminosity based on the aforementioned correlation between dust extinction and β and the observed correlation between β and $M_{UV,AB}$: $L_{\rm bol} = 10^{11.67-0.58(M_{UV,AB}+21)} L_\odot$ (though we emphasize that this relationship may not work for galaxies where $L_{\rm bol} > 10^{12} L_\odot$). We remark that it is striking that the UV LF cuts off at luminosities ($\sim$1–2 L^*_{UV}) that approximately correspond to that of ULIRGs ($\sim 10^{12} L_\odot$; see Figure 10). This suggests that L^*_{UV} at $z \sim 3$ is set by dust extinction—or more precisely the luminosity at which dust obscuration becomes so significant as to offset the increase in energy output from stars. This may explain why the value of L^*_{UV} (e.g., Steidel et al. 1999; Reddy et al. 2008) does not evolve much from $z \sim 4$ to $z \sim 2$ (see Section 5.5).
7. We correct our SFR density estimates upward to account for the contribution from dust-obscured ULIRGs. At $z \sim$ 2.5, we follow the analysis of Reddy & Steidel (2009) in using the $z \sim 2$ IR LF of Caputi et al. (2007) to account for the contribution from these galaxies and make a similar correction at $z \sim 4$ based upon $\sim$5–8 plausible submillimeter candidates at $z \sim 4$ in the HDF-North GOODS SCUBA field discussed by Daddi et al. (2009; see Section 6.2). We find that this obscured population only increases the SFR density (and dust extinction) estimates by $\sim$20% at $z \sim 2.5$ and by just $\sim$10% at $z \sim 4$ (Figure 14). Given the evolution toward bluer UV-continuum slopes β at high redshifts in both LBG and BBG selections (Section 4.2), we argue that the contribution of dust-obscured ULIRGs to the SFR density at $z \gtrsim 5$ is even less than at $z \sim 4$ (i.e., $\lesssim$ 10%). The model we construct in Section 6.2 (assuming that $L^*_{\rm bol}$ evolves similarly to L^*_{UV}) suggests that the fractional contribution of ULIRGs to the SFR density is only 6% and 2% at $z \sim 5$ and $z \sim 6$, respectively.

The distribution of UV-continuum slopes at $z \sim$ 2–6 provides us with a key window of information for studying the formation and evolution of star-forming galaxies from very early times. The very blue colors of galaxies at $z \sim$ 5–6 and at lower luminosities suggest that they are indeed much less evolved than their lower redshift or higher luminosity counterparts. These

results suggest that the dust corrections at high redshifts are not particularly large and that LBG (dropout) selections should give a substantially complete census of the SFR density at $z \gtrsim 5$ and probably even at $z \gtrsim 4$. Moreover, highly dusty galaxies seem unlikely to provide a significant contribution to the SFR density at these early times.

In the future, we expect to be able to constrain the distribution of UV-continuum slopes β at $z \sim$1–2 and $z \sim$5–8 with much more precision and accuracy than is possible at present. These advances should come using data from the *HST* WFC3/UV and WFC3/IR instrument to be installed on the *HST*. This instrument will allow us to collect deep UV data needed to efficiently select star-forming galaxies at $z \sim$1–3 and the near-IR data needed to estimate the UV-continuum slopes β for $z \sim$4–8 galaxies.

We thank Louis Bergeron, Susan Kassin, Dan Magee, Massimo Stiavelli, and Rodger Thompson for their assistance in the reduction of NICMOS data which have been essential for quantifying the UV-continuum slopes for faint star-forming galaxies at $z \sim$ 5–6. We thank Veronique Buat, Denis Burgarella, David Elbaz, Daniel Schaerer, and Naveen Reddy for stimulating conversations and Roderik Overzier and Naveen Reddy for helpful feedback on our submitted paper. Alice Shapley kindly sent us an electronic copy of her stacked spectrum of $z \sim 3$ LBGs so we could compare it against the model spectra we use to estimate the UV-continuum slopes β. We acknowledge Roelof de Jong and other scientists at STScI for their efforts at characterizing the nonlinearity in the NICMOS detector. We are appreciative to our referee for detailed and insightful feedback which greatly improved this manuscript. Finally, we believe thanks are especially due to all those at NASA, STScI and throughout the community who have worked so diligently to make Hubble the remarkable observatory that it is today. The servicing missions, like the recent SM4, have rejuvenated *HST* and made it an extraordinarily productive scientific facility time and time again, and we greatly appreciate the support of policy-makers, and all those in the flight and servicing programs who contributed to the repeated successes. We acknowledge support from NASA grants HST-GO09803.05-A and NAG5-7697.

APPENDIX

DERIVING THE UV-CONTINUUM SLOPES FROM THE OBSERVED COLORS

Here we describe our method for converting the rest-frame UV colors we measure for galaxies in our samples to their equivalent UV-continuum slopes. We base these conversions on model SEDs (Bruzual & Charlot 2003) calibrated to have UV-continuum slopes β of -2.2, -1.5, and -0.8 over the wavelength range $\sim$1600 Å to $\sim$2300 Å (to match the wavelength probed by the deep multiwavelength data available for our sample). The model SEDs assume a $e^{-t/\tau}$ star formation history, $t = 70$ Myr, $\tau = 10$ Myr, $[Z/Z_\odot] = -0.7$, and a Salpeter IMF with $E(B-V)$ dust extinction of 0.0, 0.15, and 0.3 applied using the Calzetti et al. (2000) attenuation law. We have calculated the color of these model SEDs as a function of redshift by integrating these SEDs across the filter sensitivity curves. The results are shown in Figure 15 as the solid red lines. We also have calculated the colors expected when the model SED has a perfect power-law slope $f_\lambda \propto \lambda^{-2}$ and cuts off at 912 Å (see black lines in Figure 15).

Then, knowing the effective β of the model SEDs and the observed colors of these SEDs at the mean redshift of our different dropout samples, we can derive a relation between the measured colors and the UV-continuum slope. The derived relations are

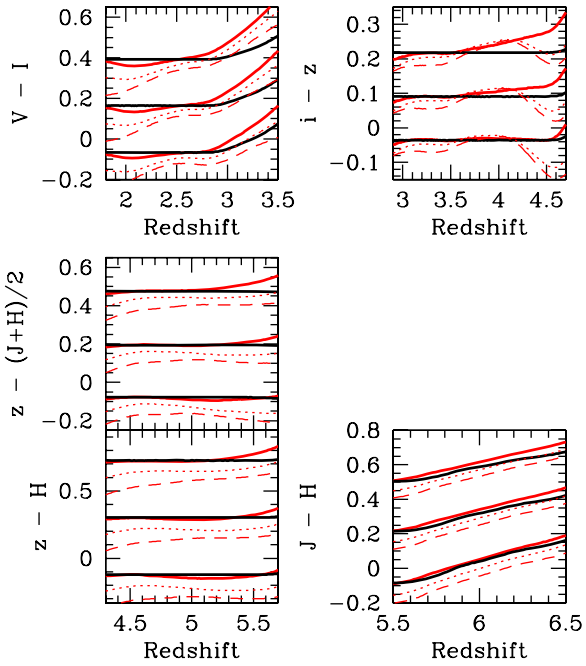

Figure 15. Expected UV colors for star-forming galaxies in our $z \sim 2.5\,U$, $z \sim 4\,B$, $z \sim 5\,V$, and $z \sim 6\,i$-dropout selections. The black lines (from bluest to reddest) correspond to power-law SEDs with β's of -2.2, -1.5, and -0.8, respectively. The red lines (from bluest to reddest) correspond to SEDs computed assuming an $e^{-t/\tau}$ star formation history, $t = 10$ Myr, $\tau = 70$ Myr, $[Z/Z_\odot] = -0.7$, the Bruzual & Charlot (2003) libraries, a Salpeter IMF, and dust extinctions $E(B-V)$ of 0.0, 0.15, and 0.3, respectively (Calzetti et al. 2000). These latter models have effective UV-continuum slopes β of -2.2, -1.5, and -0.8 over the range 1600–2300 Å —the same as the black lines. However, the red curves should be much more realistic—being based upon stellar population models (Bruzual & Charlot 2003). We reference the measured colors from each of our dropout samples to this fiducial set of SEDs (red lines) to account for intrinsic differences in the rest-frame wavelengths of the broadband imaging data available for each of our samples (Table 2 and Section 3.4). Also shown (dashed and dotted lines, respectively) are the predicted colors for SEDs computed assuming a young stellar population (a 30 Myr constant SFR model) and a somewhat older stellar population (a model for which star formation proceeded at a constant rate for 100 Myr and then ceased for 10 Myr prior to observation). Dust extinction for these alternate star formation histories is varied so that the UV-continuum slope β is equal to the same values (-2.2, -1.5, and -0.8) as for our fiducial SEDs. In general, the UV-continuum slopes β we derive from the UV colors shown here show little dependence upon the redshift of sources in our dropout samples. Small changes in the mean redshift of our selection (i.e., $\Delta z \sim 0.1$) result in shifts of $\sim$0.02, $\sim$0.02, $\sim$0.01, and $\sim$0.05 in the β's derived for our U-, B-, V-, and i-dropout selections (see the Appendix).

$$\beta = 3.04(V-I) - 1.99 \text{ (for } U-\text{dropouts)} \quad \text{(A1)}$$

$$\beta = 5.30(i-z) - 2.04 \text{ (for } B-\text{dropouts)} \quad \text{(A2)}$$

$$\beta = 2.45(z-(J+H)/2) - 1.98 \text{ (for } V-\text{dropouts with } J_{110}-\text{band data)} \quad \text{(A3)}$$

$$\beta = 1.61(z-H) - 1.96 \text{ (for } V-\text{dropouts)} \quad \text{(A4)}$$

$$\beta = 2.47(J-H) - 2.27 \text{ (for } i-\text{dropouts)}. \quad \text{(A5)}$$

The mean redshifts assumed here for our U-, B-, V-, and i-dropouts in deriving these relations are 2.5, 3.8, 5.0, and 5.9,

respectively (Bouwens et al. 2004; Bouwens et al. 2007). If the mean redshifts of our dropout selections differ from the model redshifts by $\Delta z \sim 0.1$, the derived β's would change by $\sim$0.02, $\sim$0.02, $\sim$0.01, and $\sim$0.05 with respect to those quoted here.

While the conversion formulae above were derived assuming a very plausible star formation history for $z \sim$ 2–6 galaxies, the actual star formation histories for individual galaxies in our samples likely show considerable variation. Some galaxies are likely in the midst of starbursts when we observe them, while other galaxies have likely undergone bursts some time in the past and so would have slightly older stellar populations. This results in some degree of variation in the shape of the SEDs in our samples—which is above and beyond what we can parameterize using the model SEDs above, with a simple one-parameter variation in the overall dust extinction.

To show the extent to which the observed colors depend on the assumed star formation history, in Figure 15 we also show these colors for a relatively young stellar population (with 30 Myr of constant star formation) and a somewhat older stellar population (a model for which star formation proceeded at a constant rate for 100 Myr and then ceased for 10 Myr prior to observation). Dust attenuation for these alternate star formation histories is varied so that the UV-continuum slope β is alternatively -2.2, -1.5, and -0.8. The colors of these model SEDs at the mean redshift of our dropout samples are similar to that for our fiducial model (by construction). The only exception is the $i-z$ color for our B-dropout selection which probes a slightly different wavelength range (i.e., Table 2) than the default range 1650–2300 Å.

We can attempt to use these model SEDs to estimate the approximate uncertainty in converting from the observed colors to UV-continuum slope β. Assuming the high-redshift population is composed of an equal mix of the two alternate model SEDs and our fiducial model SED and averaging over redshift, we estimate an error $\Delta\beta$ of 0.02, 0.10, 0.02, and 0.02 in the derived β's at $z \sim 2.5$, $z \sim 4$, $z \sim 5$, and $z \sim 6$.

REFERENCES

Adelberger, K. L., & Steidel, C. C. 2000, ApJ, 544, 218
Baldry, I. K., Glazebrook, K., Brinkmann, J., Ivezić, Ž., Lupton, R. H., Nichol, R. C., & Szalay, A. S. 2004, ApJ, 600, 681
Barger, A. J., Cowie, L. L., Sanders, D. B., Fulton, E., Taniguchi, Y., Sato, Y., Kawara, K., & Okuda, H. 1998, Nature, 394, 248
Bavouzet, N., Dole, H., Le Floc'h, E., Caputi, K. I., Lagache, G., & Kochanek, C. S. 2008, A&A, 479, 83
Beckwith, S. V. W., et al. 2006, AJ, 132, 1729
Bell, E. F. 2002, ApJ, 577, 150
Bertin, E., & Arnouts, S. 1996, A&AS, 117, 39
Bertoldi, F., Carilli, C. L., Cox, P., Fan, X., Strauss, M. A., Beelen, A., Omont, A., & Zylka, R. 2003, A&A, 406, L55
Blakeslee, J. P., Anderson, K. R., Meurer, G. R., Benítez, N., & Magee, D. 2003, in ASP Conf. Ser. 295, Astronomical Data Analysis Software and Systems XII, ed. H. E. Payne, R. I. Jedrzejewski, & R. N. Hook (San Francisco, CA: ASP), 257
Boone, F., Schaerer, D., Pelló, R., Combes, F., & Egami, E. 2007, A&A, 475, 513
Bouwens, R., Broadhurst, T., & Illingworth, G. 2003, ApJ, 593, 640
Bouwens, R., Broadhurst, T., & Silk, J. 1998a, ApJ, 506, 557
Bouwens, R., Broadhurst, T., & Silk, J. 1998b, ApJ, 506, 579
Bouwens, R. J., Illingworth, G. D., Blakeslee, J. P., Broadhurst, T. J., & Franx, M. 2004, ApJ, 611, L1
Bouwens, R. J., Illingworth, G. D., Blakeslee, J. P., & Franx, M. 2006, ApJ, 653, 53
Bouwens, R. J., Illingworth, G. D., Franx, M., & Ford, H. 2007, ApJ, 670, 928
Bouwens, R. J., Illingworth, G. D., Franx, M., & Ford, H. 2008, ApJ, 686, 230
Bouwens, R. J., et al. 2009a, ApJ, 690, 1764
Bouwens, R. J., et al. 2009b, ApJ, submitted (arXiv:0909:1803)
Brammer, G. B., & van Dokkum, P. G. 2007, ApJ, 654, L107
Bruzual, G., & Charlot, S. 2003, MNRAS, 344, 1000
Buat, V., Marcillac, D., Burgarella, D., Le Floc'h, E., Takeuchi, T. T., Iglesias-Paràmo, J., & Xu, C. K. 2007, A&A, 469, 19
Bunker, A. J., Stanway, E. R., Ellis, R. S., McMahon, R. G., & McCarthy, P. J. 2003, MNRAS, 342, L47
Burgarella, D., Buat, V., & Iglesias-Páramo, J. 2005, MNRAS, 360, 1413
Burgarella, D., Le Floc'h, E., Takeuchi, T. T., Huang, J. S., Buat, V., Rieke, G. H., & Tyler, K. D. 2007, MNRAS, 380, 986
Calzetti, D., Armus, L., Bohlin, R. C., Kinney, A. L., Koornneef, J., & Storchi-Bergmann, T. 2000, ApJ, 533, 682
Capak, P., et al. 2008, ApJ, 681, L53
Caputi, K. I., et al. 2007, ApJ, 660, 97
Carilli, C. L., et al. 2008, ApJ, 689, 883
Casertano, S., et al. 2000, AJ, 120, 2747
Chapman, S. C., Blain, A. W., Smail, I., & Ivison, R. J. 2005, ApJ, 622, 772
Chary, R., Berger, E., & Cowie, L. 2007a, ApJ, 671, 272
Chary, R., & Elbaz, D. 2001, ApJ, 556, 562
Chary, R.-R., Stern, D., & Eisenhardt, P. 2005, ApJ, 635, L5
Chary, R.-R., Teplitz, H. I., Dickinson, M. E., Koo, D. C., Le Floc'h, E., Marcillac, D., Papovich, C., & Stern, D. 2007b, ApJ, 665, 257
Chen, H.-W., et al. 2009, ApJ, 691, 152
Coleman, G. D., Wu, C.-C., & Weedman, D. W. 1980, ApJS, 43, 393
Condon, J. J. 1992, ARA&A, 30, 575
Cortese, L., et al. 2006, ApJ, 637, 242
Daddi, E., Cimatti, A., Renzini, A., Fontana, A., Mignoli, M., Pozzetti, L., Tozzi, P., & Zamorani, G. 2004, ApJ, 617, 746
Daddi, E., et al. 2007, ApJ, 670, 173
Daddi, E., et al. 2009, ApJ, 694, 1517
Dale, D. A., et al. 2007, ApJ, 655, 863
Dannerbauer, H., Walter, F., & Morrison, G. 2008, ApJ, 673, L127
de Jong, R. S., et al. 2006, in The 2005 HST Calibration Workshop, ed. A. Koekemoer, P. Goud Frooij, & L. L. Dressel (Baltimore, MD: STScI), 121
Dickinson, M. 1999, in AIP Conf. Proc. 470, After the Dark Ages: When Galaxies were Young (the Universe at 2 < Z < 5), ed. S. S. Holt & F. W. Olin (Melville, NY: AIP), 122
Dickinson, M., et al. 2004, ApJ, 600, L99
Dow-Hygelund, C. C., et al. 2007, ApJ, 660, 47
Dunkley, J., et al. 2009, ApJS, 180, 306
Dunlop, J. S., Cirasuolo, M., & McLure, R. J. 2007, MNRAS, 376, 1054
Dunlop, J. S., et al. 2004, MNRAS, 350, 769
Elbaz, D., et al. 2007, A&A, 468, 33
Elíasdóttir, Á., et al. 2007, arXiv:0710.5636
Erb, D. K., Shapley, A. E., Pettini, M., Steidel, C. C., Reddy, N. A., & Adelberger, K. L. 2006a, ApJ, 644, 813
Erb, D. K., Steidel, C. C., Shapley, A. E., Pettini, M., Reddy, N. A., & Adelberger, K. L. 2006b, ApJ, 647, 128
Eyles, L. P., Bunker, A. J., Ellis, R. S., Lacy, M., Stanway, E. R., Stark, D. P., & Chiu, K. 2007, MNRAS, 374, 910
Fan, X., et al. 2006, AJ, 132, 117
Ferguson, H. C., et al. 2004, ApJ, 600, L107
Förster Schreiber, N. M., et al. 2006, AJ, 131, 1891
Fruchter, A. S., et al. 2006, Nature, 441, 463
Franx, M., Illingworth, G. D., Kelson, D. D., van Dokkum, P. G., & Tran, K.-V. 1997, ApJ, 486, L75
Giavalisco, M., et al. 2004a, ApJ, 600, L93
Giavalisco, M., et al. 2004b, ApJ, 600, L103
Hathi, N. P., Malhotra, S., & Rhoads, J. E. 2008, ApJ, 673, 686
Hopkins, A. M. 2004, ApJ, 615, 209
Hopkins, A. M., & Beacom, J. F. 2006, ApJ, 651, 142
Hopkins, A. M., Connolly, A. J., Haarsma, D. B., & Cram, L. E. 2001, AJ, 122, 288
Hu, E. M., Cowie, L. L., McMahon, R. G., Capak, P., Iwamuro, F., Kneib, J.-P., Maihara, T., & Motohara, K. 2002, ApJ, 568, L75
Hughes, D. H., et al. 1998, Nature, 394, 241
Jansen, R. A., Franx, M., Fabricant, D., & Caldwell, N. 2000, ApJS, 126, 271
Jee, M. J., et al. 2007, ApJ, 661, 728
Kennicutt, R. C., Jr. 1998, ARA&A, 36, 189
Kistler, M. D., Yuksel, H., Beacom, J. F., Hopkins, A. M., & Wyithe, J. S. B. 2009, in press (arXiv:0906.0590)
Kong, X., Charlot, S., Brinchmann, J., & Fall, S. M. 2004, MNRAS, 349, 769
Kron, R. G. 1980, ApJS, 43, 305
Kroupa, P. 2001, MNRAS, 322, 231
Labbé, I., et al. 2003, AJ, 125, 1107
Labbé, I., et al. 2005, ApJ, 624, L81
Labbé, I., et al. 2007, ApJ, 665, 944
Laird, E. S., Nandra, K., Adelberger, K. L., Steidel, C. C., & Reddy, N. A. 2005, MNRAS, 359, 47
Lehmer, B. D., et al. 2005, AJ, 129, 1

Lehnert, M. D., & Bremer, M. 2003, ApJ, 593, 630
Lehnert, M. D., & Bremer, M. N. 2005, in Multiwavelength Mapping of Galaxy Formation and Evolution, ed. R. Bender & A. Renzini (Berlin: Springer), 18
Li, L.-X. 2008, MNRAS, 388, 1487
Limousin, M., et al. 2007, ApJ, 668, 643
Limousin, M., et al. 2008, A&A, 489, 23
Madau, P., Pozzetti, L., & Dickinson, M. 1998, ApJ, 498, 106
Magee, D. K., Bouwens, R. J., & Illingworth, G. D. 2007, in ASP Conf. Ser. 376, Astronomical Data Analysis Software and Systems XVI, ed. R. A. Shaw, F. Hill, & D. J. Bell (San Francisco, CA: ASP), 261
Magnelli, B., Elbaz, D., Chary, R. R., Dickinson, M., Le Borgne, D., Frayer, D. T., & Willmer, C. N. A. 2009, A&A, 496, 57
Maiolino, R. 2006, in Highlights of Astronomy Vol. 14 (XXVth IAU General Assembly, Joint Discussion 7), ed. K. A. van der Hucht (Cambridge: Cambridge Univ. Press), 17 (http://obswww.unige.ch/sfr/jd07/Proceedings/proceedings_jd07_dec06.pdf)
Maiolino, R., Schneider, R., Oliva, E., Bianchi, S., Ferrara, A., Mannucci, F., Pedani, M., & Roca Sogorb, M. 2004, Nature, 431, 533
Maiolino, R., et al. 2008, A&A, 488, 463
Mancini, C., Matute, I., Cimatti, A., Daddi, E., Dickinson, M., Rodighiero, G., Bolzonella, M., & Pozzetti, L. 2009, A&A, 500, 705
Martin, D. C., et al. 2005, ApJ, 619, L59
Meurer, G. R., Heckman, T. M., & Calzetti, D. 1999, ApJ, 521, 64
Meurer, G. R., Heckman, T. M., Lehnert, M. D., Leitherer, C., & Lowenthal, J. 1997, AJ, 114, 54
Meurer, G. R., Heckman, T. M., Leitherer, C., Kinney, A., Robert, C., & Garnett, D. R. 1995, AJ, 110, 2665
Mo, H. J., Mao, S., & White, S. D. M. 1998, MNRAS, 295, 319
Mobasher, B., et al. 2005, ApJ, 635, 832
Murphy, E. J., Chary, R.-R., Alexander, D. M., Dickinson, M., Magnelli, B., Morrison, G., Pope, A., & Teplitz, H. I. 2009, ApJ, 698, 1380
Nandra, K., Mushotzky, R. F., Arnaud, K., Steidel, C. C., Adelberger, K. L., Gardner, J. P., Teplitz, H. I., & Windhorst, R. A. 2002, ApJ, 576, 625
Oesch, P. A., et al. 2007, ApJ, 671, 1212
Oesch, P. A., et al. 2009, ApJ, 690, 1350
Oke, J. B., & Gunn, J. E. 1983, ApJ, 266, 713
Ouchi, M., et al. 2004, ApJ, 611, 660
Ouchi, M., et al. 2008, ApJS, 176, 301
Overzier, R. A., et al. 2008, ApJ, 673, 143
Panuzzo, P., Granato, G. L., Buat, V., Inoue, A. K., Silva, L., Iglesias-Páramo, J., & Bressan, A. 2007, MNRAS, 375, 640
Papovich, C., Dickinson, M., & Ferguson, H. C. 2001, ApJ, 559, 620
Papovich, C., et al. 2004, ApJ, 600, L111
Papovich, C., et al. 2006, ApJ, 640, 92
Pérez-González, P. G., et al. 2005, ApJ, 630, 82
Pickles, A. J. 1998, PASP, 110, 863
Pope, A., et al. 2006, MNRAS, 370, 1185
Prochaska, J. X., Chen, H.-W., Dessauges-Zavadsky, M., & Bloom, J. S. 2007, ApJ, 666, 267
Ranalli, P., Comastri, A., & Setti, G. 2003, A&A, 399, 39
Reddy, N. A., & Steidel, C. C. 2004, ApJ, 603, L13
Reddy, N. A., & Steidel, C. C. 2009, ApJ, 692, 778
Reddy, N. A., Steidel, C. C., Fadda, D., Yan, L., Pettini, M., Shapley, A. E., Erb, D. K., & Adelberger, K. L. 2006, ApJ, 644, 792
Reddy, N. A., Steidel, C. C., Pettini, M., Adelberger, K. L., Shapley, A. E., Erb, D. K., & Dickinson, M. 2008, ApJS, 175, 4
Riess, A. G., et al. 2007, ApJ, 659, 98
Rodighiero, G., Cimatti, A., Franceschini, A., Brusa, M., Fritz, J., & Bolzonella, M. 2007, A&A, 470, 21
Salim, S., et al. 2007, ApJS, 173, 267
Sawicki, M., & Thompson, D. 2006a, ApJ, 642, 653
Sawicki, M., & Thompson, D. 2006b, ApJ, 648, 299
Schaerer, D. 2002, A&A, 382, 28
Schaerer, D. 2003, A&A, 397, 527
Schaerer, D., & de Barros, S. 2009, A&A, 502, 705
Schaerer, D., & Pelló, R. 2005, MNRAS, 362, 1054
Schiminovich, D., et al. 2005, ApJ, 619, L47
Schinnerer, E., et al. 2008, ApJ, 689, L5
Seibert, M., Heckman, T. M., & Meurer, G. R. 2002, AJ, 124, 46
Shapley, A. E., Steidel, C. C., Pettini, M., & Adelberger, K. L. 2003, ApJ, 588, 65
Shimasaku, K., Ouchi, M., Furusawa, H., Yoshida, M., Kashikawa, N., & Okamura, S. 2005, PASJ, 57, 447
Siana, B., Teplitz, H. I., Chary, R.-R., Colbert, J., & Frayer, D. T. 2008, ApJ, 689, 59
Siana, B., et al. 2009, ApJ, 698, 1273
Sirianni, M., et al. 2005, PASP, 117, 1049
Stanway, E. R., McMahon, R. G., & Bunker, A. J. 2005, MNRAS, 359, 1184
Stanway, E. R., et al. 2007, MNRAS, 376, 727
Stark, D. P., Bunker, A. J., Ellis, R. S., Eyles, L. P., & Lacy, M. 2007, ApJ, 659, 84
Stark, D. P., Ellis, R. S., Bunker, A., Bundy, K., Targett, T., Benson, A., & Lacy, M. 2009, ApJ, 697, 1493
Steidel, C. C., Adelberger, K. L., Giavalisco, M., Dickinson, M., & Pettini, M. 1999, ApJ, 519, 1
Steidel, C. C., Giavalisco, M., Pettini, M., Dickinson, M., & Adelberger, K. L. 1996, ApJ, 462, L17
Szalay, A. S., Connolly, A. J., & Szokoly, G. P. 1999, AJ, 117, 68
Tanaka, M., Kodama, T., Arimoto, N., Okamura, S., Umetsu, K., Shimasaku, K., Tanaka, I., & Yamada, T. 2005, MNRAS, 362, 268
Thompson, R. I., Storrie-Lombardi, L. J., Weymann, R. J., Rieke, M. J., Schneider, G., Stobie, E., & Lytle, D. 1999, AJ, 117, 17
Thompson, R. I., et al. 2005, AJ, 130, 1
Tremonti, C. A., et al. 2004, ApJ, 613, 898
Treyer, M., et al. 2007, ApJS, 173, 256
van Dokkum, P. G., et al. 2006, ApJ, 638, L59
Vanzella, E., et al. 2006, A&A, 454, 423
Vanzella, E., et al. 2009, ApJ, 695, 1163
Venkatesan, A., Tumlinson, J., & Shull, J. M. 2003, ApJ, 584, 621
Verma, A., Lehnert, M. D., Förster Schreiber, N. M., Bremer, M. N., & Douglas, L. 2007, MNRAS, 377, 1024
Wang, W.-H., Barger, A. J., & Cowie, L. L. 2009, ApJ, 690, 319
Wang, B., & Heckman, T. M. 1996, ApJ, 457, 645
Wiklind, T., Dickinson, M., Ferguson, H. C., Giavalisco, M., Mobasher, B., Grogin, N. A., & Panagia, N. 2008, ApJ, 676, 781
Wilkins, S. M., Trentham, N., & Hopkins, A. M. 2008, MNRAS, 385, 687
Williams, R. E., et al. 1996, AJ, 112, 1335
Wyder, T. K., et al. 2007, ApJS, 173, 293
Yan, H., Dickinson, M., Giavalisco, M., Stern, D., Eisenhardt, P. R. M., & Ferguson, H. C. 2006, ApJ, 651, 24
Yan, H., & Windhorst, R. A. 2004, ApJ, 612, L93
Yan, H., et al. 2005, ApJ, 634, 109
Yoshida, M., et al. 2006, ApJ, 653, 988
Yüksel, H., Kistler, M. D., Beacom, J. F., & Hopkins, A. M. 2008, ApJ, 683, L5
Yun, M. S., Reddy, N. A., & Condon, J. J. 2001, ApJ, 554, 803
Zackrisson, E., Bergvall, N., & Leitet, E. 2008, ApJ, 676, L9
Zheng, X. Z., Dole, H., Bell, E. F., Le Floc'h, E., Rieke, G. H., Rix, H.-W., & Schiminovich, D. 2007, ApJ, 670, 301
Zheng, W., et al. 2009, ApJ, 697, 1907